Origin of type II diamonds

by

Korolev N.

Research report
[1.07.2016 – 1.07.2017]

The study was funded by the Dr. Eduard Gübelin Association through the 2015 Dr. Eduard Gübelin research scholarship

The University of British Columbia

(Vancouver, Canada)

July 2017

Table of Contents

List of mineral abbreviation 3
Abstract 4
1. Samples 4
2. Analytical methods 4
2.1. Fourier transform infrared spectroscopy (FTIR) 4
2.2. Electron probe microanalysis (EPMA) and cathodoluminescence 5
2.3. Raman spectroscopy 5
2.4. Laser ablation inductively coupled plasma mass spectrometry (LA-ICP-MS) 5
2.5. Secondary Ion Mass Spectrometry (SIMS) for $\delta^{13}C$ analysis 6
2.6. Fluorescence of diamonds 6
2.7. X-ray single-crystal study 6
3. Diamond morphology 7
4. UV-Fluorescence of diamonds. 9
5. FTIR study and nitrogen characteristics. 13
6. Composition of carbon isotopes 15
7. Inclusions in diamonds 18
Garnets (non majoritic) 19
Clinopyroxene 21
Orthopyroxene 25
Olivine 25
CaSiO3 (Ca-Perovskite and wollastonite) 26
Majorite 27
Coesite 27
Spinel 27
Kyanite 27
Sulphides 27
Secondary minerals 27
8. Thermobarometry 28
9. Conclusions and results 32
10. Publications and results dissemination 32
References 33
References [in the Electronic Supplementary Materials] 36
Appendix A. 37

List of mineral abbreviation

Alm	–	Almandine
Aug	–	Augite
Co	–	Coesite
Cpx	–	Clinopyroxene
Di	–	Diopside
En	–	Enstatite
Grs	–	Grossular
Ky	–	Kyanite
Mj	–	Majorite
Ol	–	Olivine
Omp	–	Omphacite
Prp	–	Pyrope
Prv	–	Perovskite
Spl	–	Spinel
Wo	–	Wollastonite

Abstract

I studied 341 diamonds (+3-11, Clivage, Breakage, Gem Quality and Melee classes) with mineral inclusions from the Cullinan mine. The report presents data on morphology, N content and aggregation state, and compositions of inclusions analyzed with Infrared (FTIR) and Raman spectroscopy, microprobe (EPMA) and laser ablation inductively coupled plasma mass-spectrometry (LA-ICP-MS). FTIR study is shown that the studied diamonds include 266 type-I and 75 type-II stones. Raman and EPMA study demonstrated a variety of primary mineral inclusions, i.e. garnet, majorite, clinopyroxene, orthopyroxene, olivine, CaSiO3 phases, coesite, spinel and kyanite. For the first time, an inclusion with a Ca-perovskite crystal structure determined by Raman spectroscopy was found. A detailed mineralogical description of inclusions and parageneses is given. All inclusions (n=201 from 119 diamonds) can be subdivided into four parageneses, lithospheric peridotitic (1) and eclogitic (2), sublithospheric mafic (3) and undetermined, represented by Fe and Fe-Ni sulphides (4). More than two thirds of the inclusions show PT-parameters consistent with the lithospheric conductive thermal regime, 1090-1400°C and 45-63 kb. Less than one third of the inclusions yields temperatures higher than the upper mantle adiabat. The sublithospheric mafic diamonds are sourced from the transition zone, based on the stability of Ca-Si perovskite (below 500 km) and the 370-445 km inferred depth of the majorite origin. Lithospheric peridotitic paragenesis predominate in Type II diamonds whereas 73% Type I stones are sourced from eclogites. Another contrast between Type II and Type I stones is the higher abundance of sublithospheric inclusions in the former, indicating the more common derivation from the transition zone,

1. Samples

The studied diamonds from the Cullinan mine were donated to the Diamond Exploration Laboratory (the University of British Columbia) by PETRA Diamonds, the company operating the Cullinan mine. The collection of diamonds consists of 341 stone. FTIR analysis has identified 75 stones as type-II diamonds (with N contents below 20 ppm) and 266 samples as type-I diamonds.

2. Analytical methods

2.1. Fourier transform infrared spectroscopy (FTIR)

Infrared spectra were collected for 341 samples (Vancouver, Canada) on a Nicolet 6700 Fourier transform infrared spectrometer. Each sample's absorbance spectra were measured at maximum light transmission. Background spectra were collected for 120 s prior to the analysis of each sample and were subtracted from each measured absorbance spectra. Count times for spectra were 40 seconds at a spectral resolution of 0.5 cm^{-1}. The nitrogen concentration and aggregation were determined by the procedure described in (Mendelssohn and Milledge, 1995) using the spreadsheet ("FTIR analyser 3d") provided by John Chapman (Rio Tinto Diamonds Ltd.). Preliminary processing and baseline determination were made using EssentialFTIR® software. The uncertainties of the analysed nitrogen concentration and aggregation state vary. Samples with flat baselines and low or moderate N concentrations approximately up to 120 ppm

gave good fits to the modeled curves and lower uncertainties, but samples with high N concentrations or complex crystal shapes yielded uneven baselines and less reliable N estimates. The analytical and processing error for the former samples is ±10%, for samples with high N concentrations (above 300 ppm N) is up to ±20%, and %IaB is ±15% (1 sigma, relative error).

2.2. Electron probe microanalysis (EPMA) and cathodoluminescence

One hundred and thirty three diamonds were polished using a diamond-impregnated steel scaife to expose individual mineral inclusions. One hundred and twelve diamonds contain inclusions which sizes are sufficient for analysis. Thus 187 inclusions from 112 diamonds (including 70 minerals from 36 type-II diamonds) have been studied.

Quantitative chemical analyses were undertaken on a CAMECA SX-50 electron microprobe (University of British Columbia, Department of Earth, Ocean and Atmospheric Sciences, Vancouver, Canada). All inclusions were coated with carbon. All elements were analyzed with a beam current of 20 nA, an acceleration voltage of 15 kV, a peak count time of 20s and two 10s backgrounds. Detection limits for most oxides were below 0.08 wt.%, detection limits for Cr_2O_3, MnO_2, and NiO were less than 0.11 wt.%. Fe^{3+} content was calculated stoichiometrically on the basis of the ideal oxygen unit total for each respective mineral. More than eight hundred EPMA points have been analyzed.

The cathodoluminescence SEM images (CL) were examined using a Philips XL 30 scanning electron microscope with a CL attachment consisting of a Hamamatsu R376 photomultiplier tube (University of British Columbia, Department of Earth, Ocean and Atmospheric Sciences, Vancouver, Canada). The accelerating voltage was 20 keV and the electron beam current was 100 μA.

2.3. Raman spectroscopy

Raman spectra were obtained with a Horiba XploRA PLUS confocal Raman spectrometer equipped with a CCD-detector at the University of British Columbia, Vancouver, Canada. Spectra were excited at room temperature with the 532.18 nm line of a 14-mW Nd-YAG laser through an OLYMPUSTM 100X objective. Raman spectra were collected between 100 and 1500-1800 cm^{-1} at 1.3 cm^{-1} spectra resolution and ~ 1 μm spatial resolution. Confocal hole was 200 μm, spectra slit width was 300 μm. More than 300 inclusions were studied by Raman spectroscopy.

Micro-Raman spectroscopy. Uninverted Ca-Si-perovskite inclusion from Cln-77 diamond was analysed by a Thermo Scientific DXR micro-Raman spectrometer installed at the Department of Chemical Sciences of University of Padova (Italy). A 532 nm excitation laser was used at a power of 3-5 mW to avoid any possible beam damage to the crystal. The Raman spectrum of Ca-Prv inclusion was collected for 30-40 seconds using a 50x objective with a spatial resolution of 1.1 μm and a spectral resolution estimated to be 2.5 cm^{-1}. The spectrum was collected between 200 and 1200 cm^{-1}.

2.4. Laser ablation inductively coupled plasma mass spectrometry (LA-ICP-MS)

Laser ablation inductively coupled plasma mass spectrometry (LA-ICP-MS) of olivine inclusions in diamond was performed at the Arctic Resources Laboratory, University of Alberta. A RESOlution 193 nm ArF excimer laser ablation system coupled to a Thermo Scientific ELEMENT XR mass spectrometer was used. Helium was used as the transport gas with a flow

rate of 1 L/min. The laser was operated at a fluence of ~4.5 J/cm^2 and a repetition rate of 5 Hz. The Argon plasma was tuned while ablating a 33 μm line on the NIST SRM 612 reference glass (at 10 Hz), so that La > 350,000 cps, Th > 500,000 cps, and ThO/Th < 0.2 %. Before each measurement, the background (gas blank) was measured for 45 s. The ablation time was 45 s, followed by 35 s wash out time. Laser spot sizes of 75 μm, 50 μm, and 33 μm were used, depending on sample size. The samples were bracketed by three analyses each of NIST SRM 612 and the in-house olivine standard SC-GB (Bussweiler et al. 2017). The isotopes 7Li, 23Na, 27Al, 31P, 43Ca, 44Ca, 45Sc, 53Cr, 55Mn, 59Co, 60Ni, 63Cu, 69Ga, 71Ga, 93Nb, 140Ce were measured in low resolution (M/ΔM = 300). 29Si was used as the internal standard. The raw data were processed in Iolite (Paton et al. 2011). Results processed with NIST SRM 612 and SC-GB are usually within 10%. However, especially for small spot sizes (e.g., 33 μm) SC-GB is the preferred calibration material because matrix-matched calibration reduces fractionation effects. Eighteen inclusions from seventeen diamonds (25 points) were studied by LA-ICP-MS.

2.5. Secondary Ion Mass Spectrometry (SIMS) for $\delta^{13}C$ analysis

Carbon isotopes ($\delta^{13}C$) were determined using Cameca IMS 7f-GEO secondary ion mass spectrometer (Caltech, USA). Polished diamond (sample cln-77) was pressed into an indium mount with a 1" diameter aluminum holder. Natural reference diamonds with a reference value $\delta^{13}C$ = -13.6‰ (2σ=0.3) and -2.5-2.6‰ (2σ=0.3) were used to determine the instrumental mass fractionation and drift before and after sample analyses. Diamonds were coated with gold (20 nm). Analyses were conducted using $^{133}Cs^+$ at 10 keV impact energy, beam current of ~4 nA. The 15 μm diameter $^{133}Cs^+$ primary-ion beam was used for pre-sputtering. During analysis, the ion beam diameter was reduced to 5 μm. Secondary ions of ^{12}C and ^{13}C were extracted at -9 keV. No e-gun charging compensation needed. Secondary ion energy bandwidth was 90 eV. $^{13}C^-/^{12}C^-$ ratios were measured using dual Faraday cups (FC1 for $^{12}C^-$ and FC2 for $^{13}C^-$). Mass Resolving power = 2900. The ^{12}C as well as ^{13}C ions were counted for 1 second, in each cycle (30 cycles in total). Total time spent on each spot was 8 minutes. The standard deviation of the analyses is about 0.4 to 0.5 ‰ at the two-sigma level.

2.6. Fluorescence of diamonds

Diamond fluorescence was examined using a 100 watt ultraviolet bulb attached to a Leica MZ FLIII stereomicroscope and powered by an EBQ Netz power source. A Spot Insight Color 3.2.0. digital camera was used to record images. Exposure time of twenty seconds was used to collect most of images. For some samples with very high or low FL intensity exposure time varied from 5 to 35 seconds.

Through comparison of FL digital photographs of diamonds, stones are described in terms of: colour, homogeneity and intensity. Each homogeneous diamond is grouped into one of the four FL colours group (blue, turquoise, green and colorless) and is qualitatively rated in terms of relative intensity (strong, moderate, weak or very weak).

2.7. X-ray single-crystal study

Ca-Prv inclusion from cln-77 diamond was examined using the single crystal diffractometry. Rigaku-Oxford Diffraction Supernova single-crystal diffractometer (Kappa-geometry) equipped with an X-ray micro-source (MoKα wavelength; beam spot ~ 120 μm) and a 200K Pilatus detector (Dectris) was used. The instrumentation, installed at the Department of

Geosciences of University of Padova, still a prototype, was assembled specifically to study very small inclusions within their diamond hosts. After several attempts to center the inclusion under the X-ray beam 91 reflections were measured, which were merged into only 9 unique reflections. The 91 reflections were processed in the Crysalis software (Rigaku-Oxford Diffraction) to obtain the unit-cell parameters.

3. Diamond morphology

The morphology of the diamonds, together with the degree of resorption and color, were studied with a binocular microscope and documented in Electronic Supplementary Material 1 (ESM 1).

Diamonds for the study were selected from the run-of-the-mine production from classes: comm/boart 2-2.5 (breakage) ct, 5-10 ct (breakage) and +10.8 ct (breakage); clivage –5+3, –11+9 and 5-10 ct (breakage); melee –3+1, –9+5 and –11+9; and gem quality –5+3 and –9+5. Because of this, the morphology, the color and the sizes of the original selection were very limited.

Diamonds with weight between 0.01-0.07 ct. are predominate (87%) (Fig. 1). The biggest diamonds have weight 0.2-0.34 ct. and amount to 2% of all stones (n=8). Most of stones are represented by single crystals or fragment of crystals (Table 1). Share of macles and aggregates is less than 14%. It's also valid for the type II diamonds. Approximately 70% of all stones and 59% of type II diamonds have dodecahedral habit (Table 2). Other observed shapes of crystals: octahedral (with transitional between octahedron and dodecahedroid forms and flatted octahedral habit) and hemimorphic crystals (Table 2). Diamond resorption degree was ranked from 1 (no remaining octahedral faces to 6 (unresorbed) according to the scale (McCallum et al., 1994). With respect to the classification by morphology, diamonds in resorbtion classes 1 and 2 were classified as dodecahedra, whereas categories 3-6 were classified as octahedral. Thus, the majority of diamonds has resorption categories 1 and 2 (Table 3). Color was evaluated visually by a binocular microscope. Forty six diamonds have strongly marked brown color of different shades. Other colors were not recognized. Many crystals show various surface morphology features (ESM 1), the most common of them being etch channels and figures, trigonal and hexagonal etch pits, caverns, trigonal layers, steps of growth on the edges, sheaf-like striation, tile-columnar sculpture, block sculpture and shargreen relief. Green pigmentation spots were found on the surface of eight type-I diamonds.

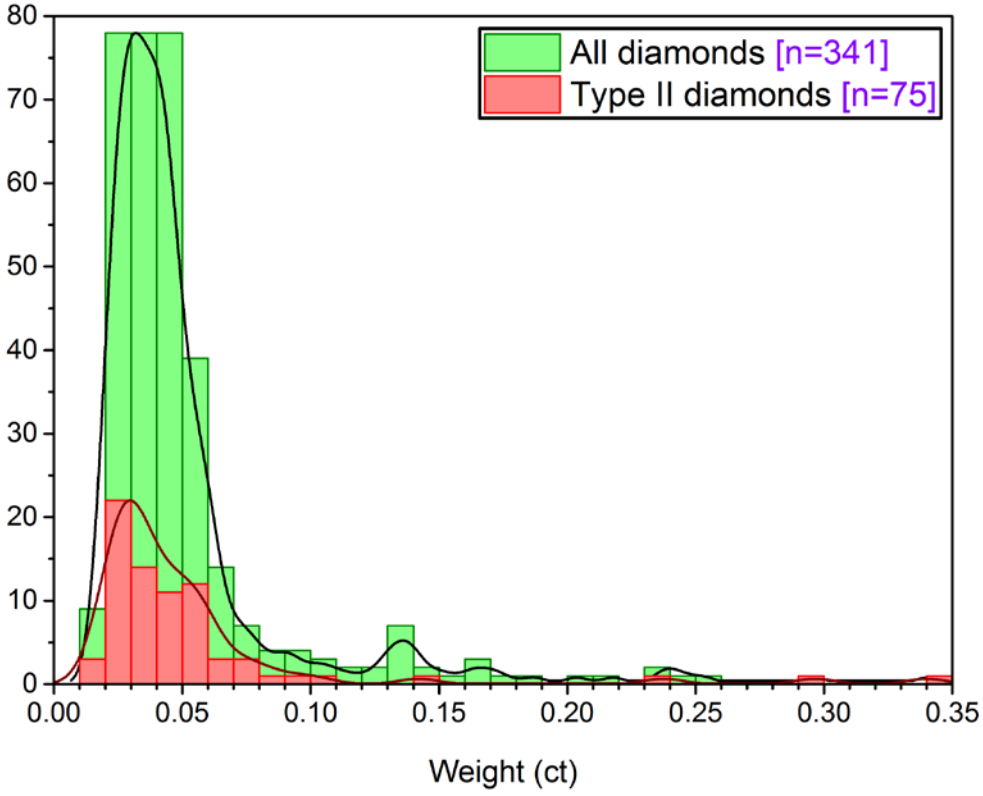

Fig. 1. Distribution of the studied Cullinan mine diamond weights. Lines are distribution curves (kernel smoothed).

Table 1. Fragmentation of the studied Cullinan mine diamonds.

Fragmentation	**Type-I**		**Type-II**		**Total**	
	N (diamonds)	**N (diamonds) (%)**	**N (diamonds)**	**N (diamonds) (%)**	**N (diamonds)**	**N (diamonds) (%)**
Crystal (chipped crystal)	180	68	44	59	224	66
Fragment of crystal	55	12	12	16	67	20
Macle (chipped macle)	2	1	6	8	8	2
Aggregate of 2 crystals	28	11	10	13	38	11
Aggregate of 3 crystals	1	0	3	4	4	1
Total:	266	100	75	100	341	100

Table 2. Type of the studied Cullinan mine diamond habits.

Type of diamond habits	**Type-I**		**Type-II**		**Total**	
	N (diamonds)	**N (diamonds) (%)**	**N (diamonds)**	**N (diamonds) (%)**	**N (diamonds)**	**N (diamonds) (%)**
Octahedral	41	15.5	24	32	65	19
Dodecahedral	194	73	44	59	238	70
Hemimorphic	6	2	0	0	6	2
Unrecognizable	25	9.5	7	9	32	9
Total:	266	100	75	100	341	100

Table 3. Resorption categories of the studied Cullinan mine diamonds.

Resorption class	Type-I		Type-II		Total	
	N (diamonds)	N (diamonds) (%)	N (diamonds)	N (diamonds) (%)	N (diamonds)	N (diamonds) (%)
1	198	74	47	63	245	72
2	5	2	0	0	5	1
3	11	4	1	1	12	3
4	10	4	6	8	16	5
5	12	5	11	15	23	7
6	9	3	6	8	15	4
Unrecognizable and hemimorphic	21	8	4	5	25	8
Total:	266	100	75	100	341	100

4. UV-Fluorescence of diamonds.

All 341 samples were examined under ultraviolet light. There is a strong contrast between FL colours and relative colour intensity distribution of type-I and type-II diamonds. 90.7% (n=68) of type-II diamonds have no FL colour. The other part is represented by diamonds with blue FL colour of weak or very weak intensity (5.4%, n=4), green FL colour of weak intensity (1.3%, n=1) and two (2.7%) heterogeneous stones with blue and green colours (table 4, fig. 2 and 3). At the same time, 51.9% of type-I diamonds have FL blue (35.8%), turquoise (15%) and green (0.4%) colours of different intensity (table 4, fig. 2-5). A summary of the results is presented in ESM 2.

Table 4. Fluorescence colours and relative intensity distribution (%) of Cullinan type-I and type-II diamonds.

Type I (n=266)					
Intensity	**Blue**	**Turquoise**	**Green**	**No fluorescence**	**Heterogeneous**
Strong	11.7	4.5	-	48.1	0.8
Moderate	9.8	4.5	0.4		
Weak	6.4	1.9	-		
Very weak	7.9	4.1	-		
Total	35.8	15.0	0.4	48.1	0.8
Type II (n=75)					
Intensity	**Blue**	**Turquoise**	**Green**	**No fluorescence**	**Heterogeneous**
Strong	-	-	-	90.7	2.7 blue and green
Moderate	-	-	-		
Weak	2.7	-	-		
Very weak	2.7	-	1.3		
Total	5.4	-	1.3	90.7	2.7

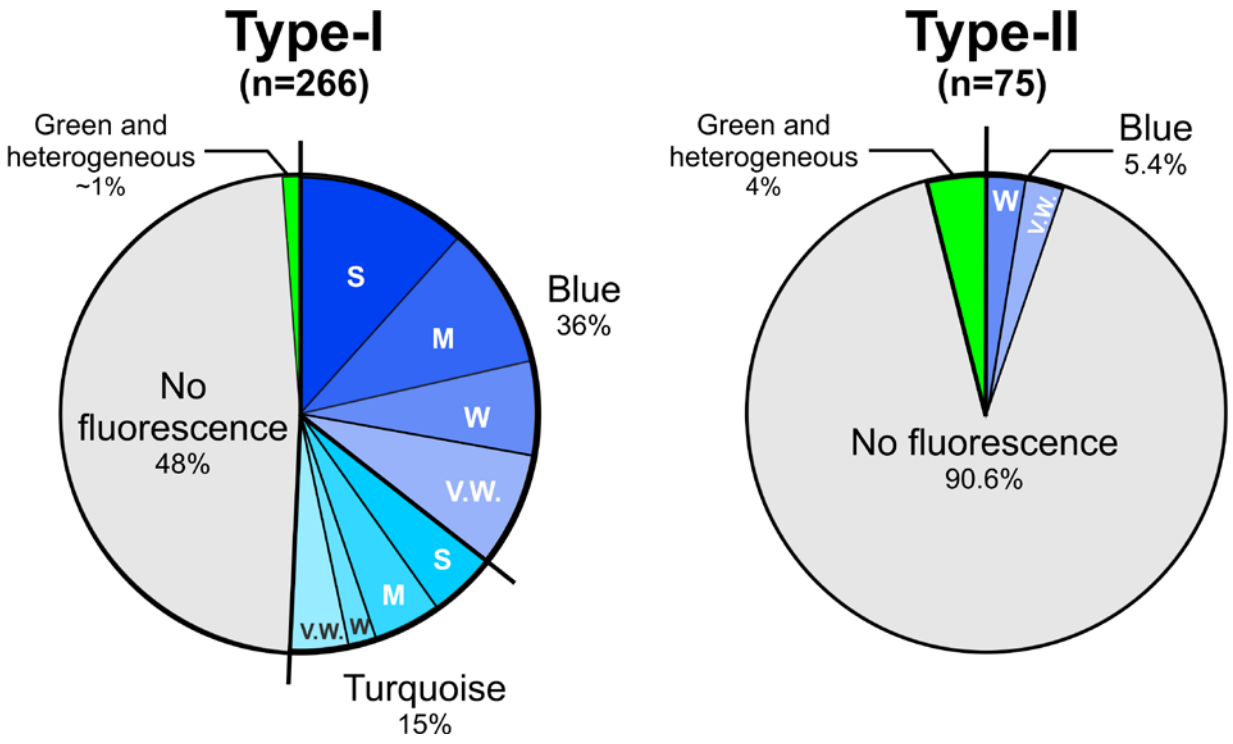

Fig. 2. Fluorescence colours and relative intensity (S - strong, M -moderate, W - weak or V.W. - very weak) distribution of Cullinan type-I and type-II diamonds.

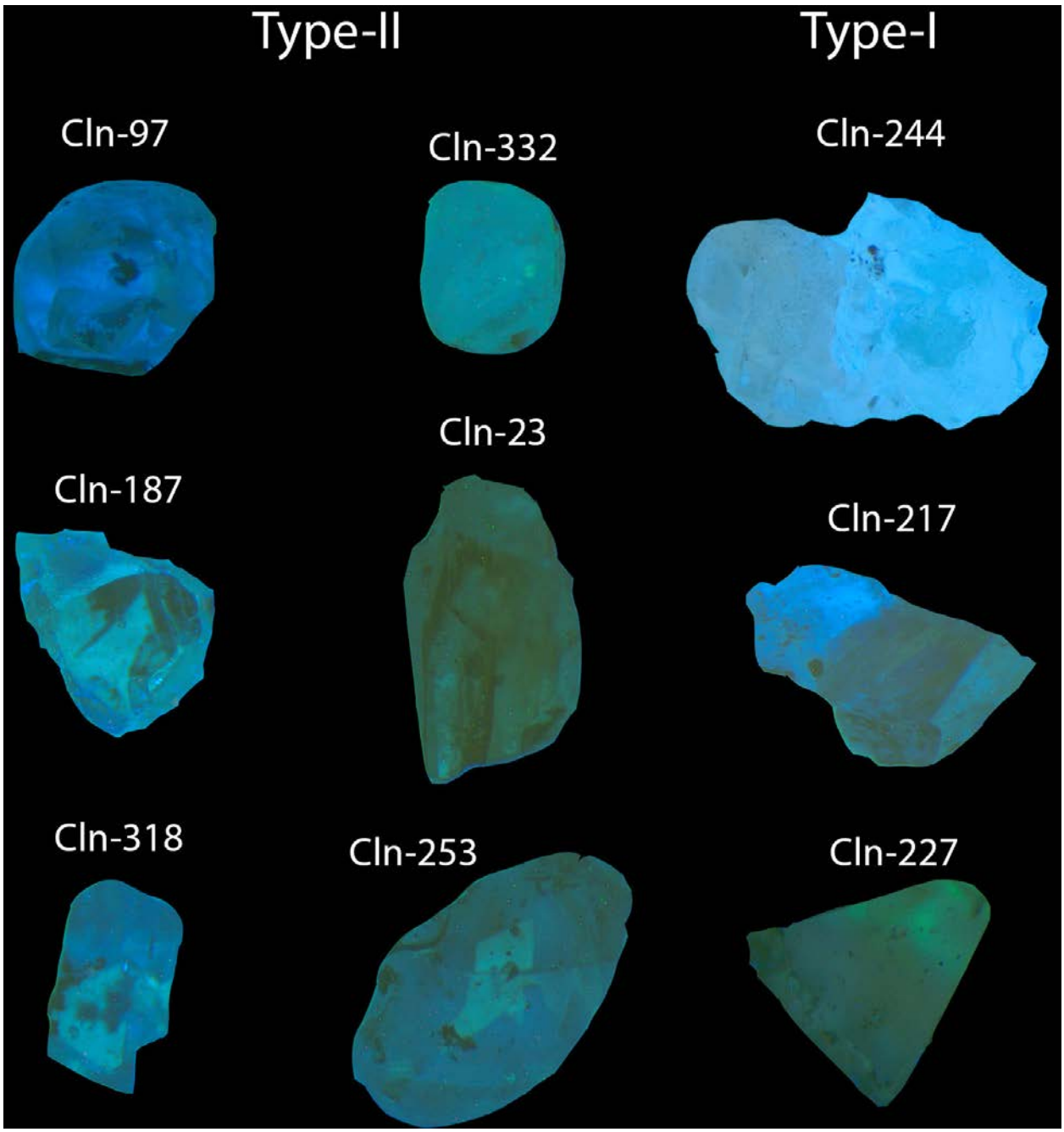

Fig. 3. Photographs of various FL colours observed for Cullinan type-II homo- and heterogeneous and type-I heterogeneous diamonds.

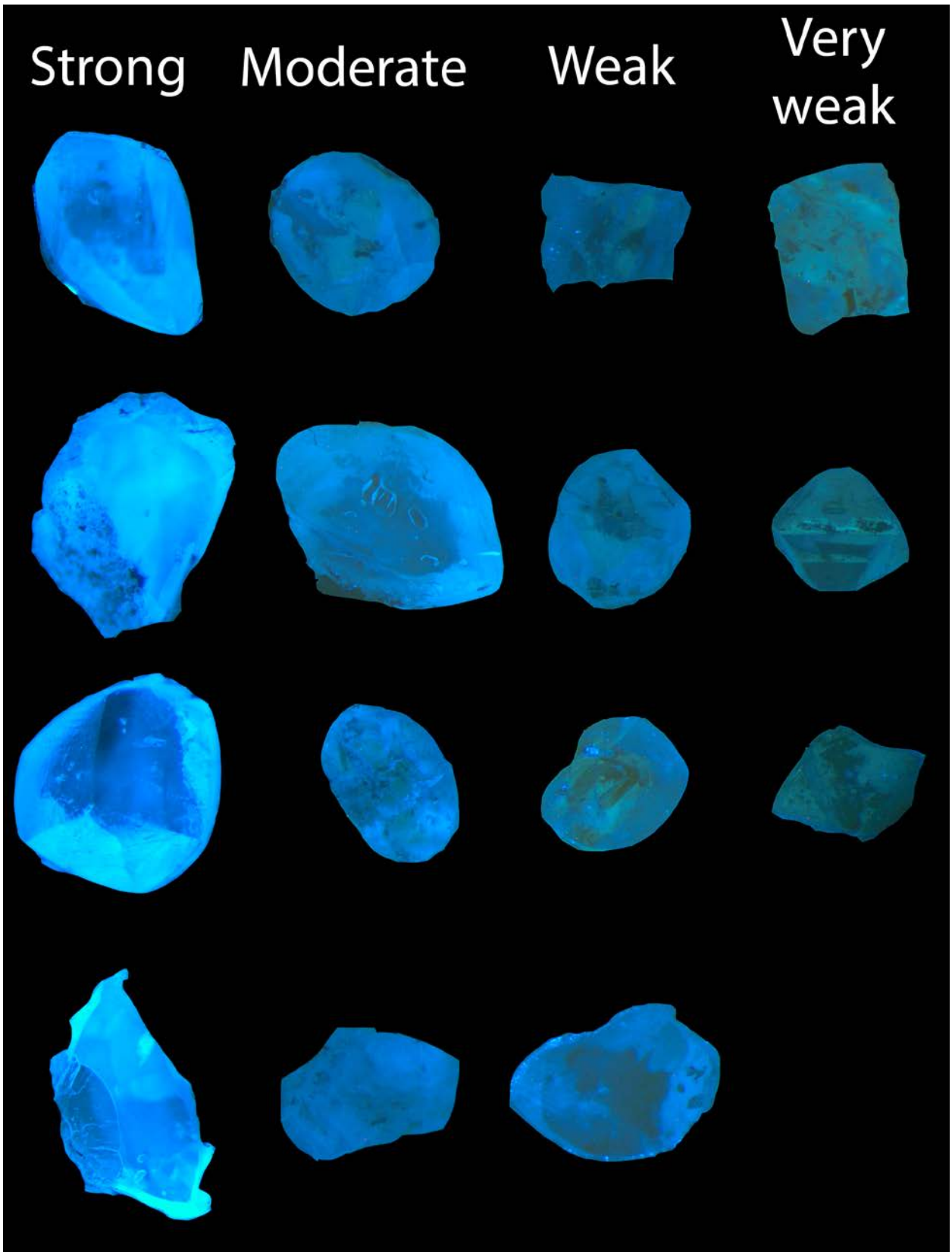

Fig. 4. Representative photographs of various FL blue colours intensity observed for Cullinan type-I homogeneous diamonds.

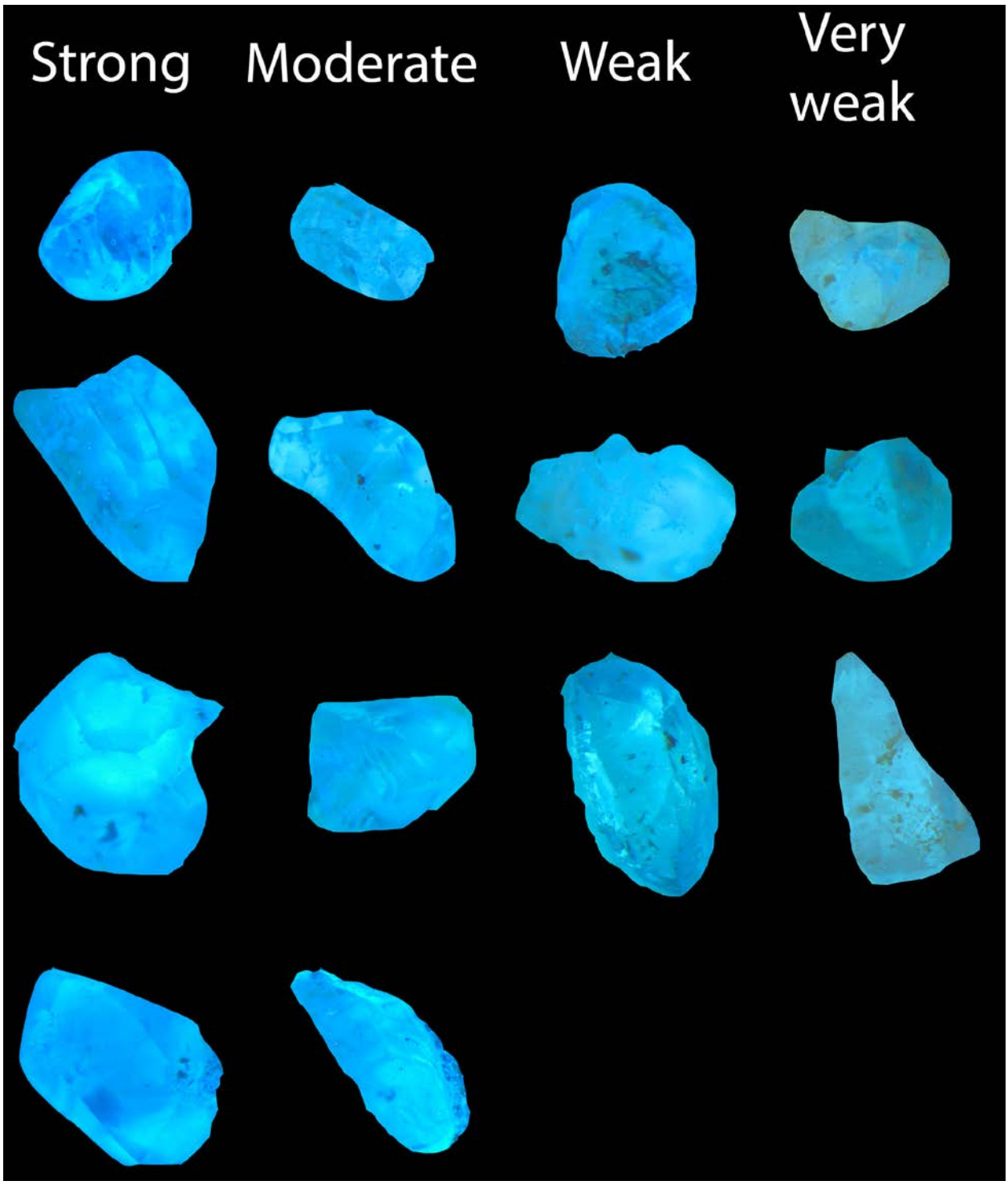

Fig. 5. Representative photographs of various FL turquoise colours intensity observed for Cullinan type-I homogeneous diamonds.

5. FTIR study and nitrogen characteristics.

FTIR study is shown that the studied Cullinan mine diamonds include 204 IaB, 54 IaAB, 8 IaA and 75 type-II stones. Representative spectra of each type are demonstrated on Fig. 6. Total calculated N concentration varies from 0 to 720 ppm (Fig. 7), with an average and median of type-II diamonds 10 and 10 ppm, and type-I diamonds 210 and 175 ppm accordingly. The degree to which total nitrogen is aggregated into B-centers in type-I diamonds (denoted hereafter

as %IaB) ranges from 7.4 to 100% with an average and median 76 and 86. It clearly shows that most of the nitrogen is aggregated into B-centers and quite rarely into A-centers. It should be noted that no linear correlation is present between calculated total nitrogen concentration and %IaB (r= -0.06). We didn't find a correlation between the nitrogen concentration in diamonds and their morphological characteristics or the chemical composition of inclusions. All spectra of type-I diamonds show a peak at 3107 cm^{-1} assigned to hydrogen impurity. At the same time the absorption peak at 3107 cm^{-1} is absent in 25 spectra of type-II diamond. Often type-I and II diamond IR-spectra demonstrate group of peaks at 2850, 2920 and 2960 cm^{-1}, which correspond to the symmetric and asymmetric stretch bands of CH_2 group (Titus et al., 2005), the apparent CO_2 band at 2350-2360 cm^{-1} and water peaks. Boron impurities were not found. Nitrogen contents and other FTIR characteristics of diamonds are given in Electronic Supplementary Material (ESM 2).

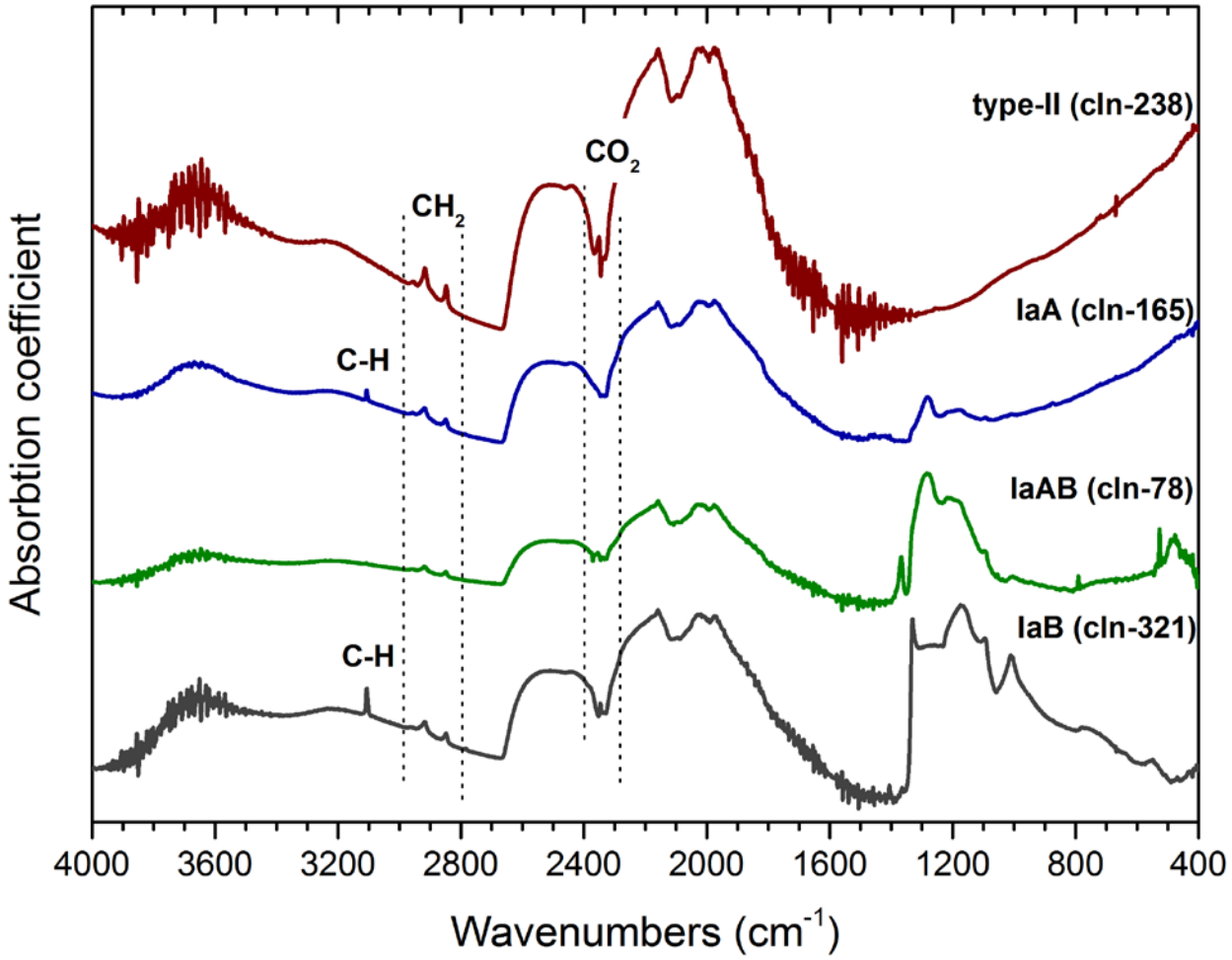

Fig. 6. FTIR absorption spectra of 4 representative diamond samples from the Cullinan mine collection.

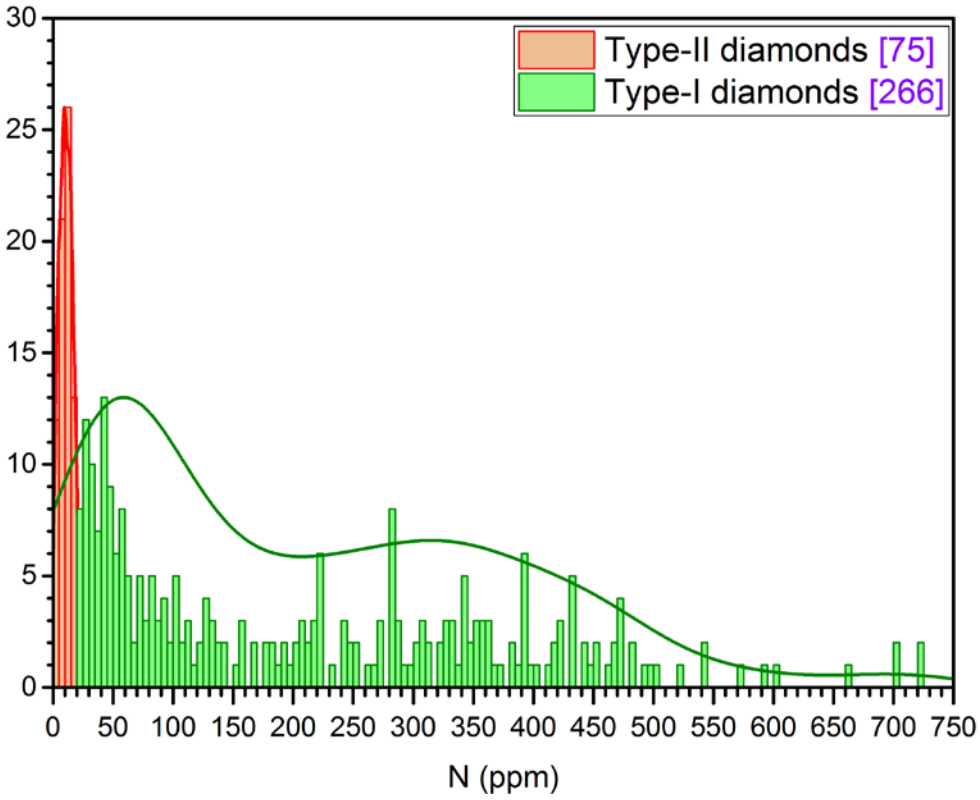

Fig. 7. Variations of nitrogen contents in the studied Cullinan mine diamonds. Green line is a distribution curve (kernel smoothed) for Type I diamonds.

6. Composition of carbon isotopes

Carbon isotopic composition ($\delta^{13}C$) of 45 diamonds was determined with SIMS spot analyses (94 spots) (Table 5, Figures 8 and 9). Representative cathodoluminescence (CL) images of type-I and type-II polished diamonds from Cullinan pipe with spots of carbon isotope analysis are shown in the Appendix A. $\delta^{13}C$ range of type-I diamond from -2.1 to -7.7‰ with a mean -4.5‰ (n=25). $\delta^{13}C$ range of type-II diamond from -1.3 to -7.8‰ with a mean -3.8‰ (n=20). Obtained carbon isotopic data and quite narrow $\delta^{13}C$ range -1.3– -7.8 (n=45) for different type of Cullinan diamonds are consistent with previous datasets (Deines et al., 1984, 1989; Deines, Harris, 1995; Viljoen et al., 2004).

Type-I diamonds with the lithospheric eclogitic inclusions have a very narrow $\delta^{13}C$ range -4.4 – -4.8‰ (n=8) (fig. 8), excluding one diamond with a grospydite association (grossular + diopside) with $\delta^{13}C$ -3.6‰. Type-II diamonds with coesite inclusions have the highest values of $\delta^{13}C$ -2.1– -2.6‰ (n=4, associations: Mj+Co+Ky, Co+Ky, Omp+Co, En+Co, Table 5). Other dependences between $\delta^{13}C$ and type of inclusions or diamonds were not brought out. Additionally, any dependence between $\delta^{13}C$ and nitrogen contents in diamonds and type of paragenesis or type of diamond habits also was not found (Table 5, Figures 8 and 9).

Table 5. Carbon isotope composition of type-I and type-II diamonds from Premier pipe. Type of mineral inclusion is pointed out in the square brackets. Diamonds of dodecahedral habit are highlighted in light green; diamonds of octahedral habit are highlighted in red. Diamonds of unrecognizable habit are not highlighted. Omp^{min} – clinopyroxene inclusion with minimum contents of omphacite end member, Omp^{max} - clinopyroxene inclusion with maximum contents of omphacite end member.

N	Sublithospheric mafic						Lithospheric eclogitic						Lithospheric peridotitic					
	Type I	$\delta^{13}C$ Core	$\delta^{13}C$ Rim	Type II	$\delta^{13}C$ Core	$\delta^{13}C$ rim	Type I	$\delta^{13}C$ Core	$\delta^{13}C$ rim	Type II	$\delta^{13}C$ Core	$\delta^{13}C$ rim	Type I	$\delta^{13}C$ Core	$\delta^{13}C$ rim	Type II	$\delta^{13}C$ Core	$\delta^{13}C$ rim
1	**77** [Prv]	-4.6	-2.4 / -3.9	**79** [Wo]	-1.8		**145** [Grs+Di]	-3.6	-4.1	**8** [Co+Ky]	-2.6	-4.3	**33** [Ol]	-5.0	-4.7	**233** [Ol]	-6.8	
2	**67** [Mj+Omp]	-3.3	-5.4	**85** [Mj+Omp]	-4.4		**106** [Prp+Cpx]	-4.6	-4.6	**62** [Omp+ Co]	-2.4	-3.8	**294** [Ol]	-3.1	-2.8	**341** [Ol]	-6.8	-6.7
3	**218** [Mj+Prp]	-2.1	-4.2	**292** [Mj]	-4.3		**306** [Prp+Omp]	-4.6	-3.3	**181** [Omp+ Aug]	-4.2	-4.2	**34** [Ol_3]	-6.4	-7.1	**335** [Ol]	-3.2	
4	**297** [Mj+Omp]	-4.2	-4.2	**171** [Mj+Co+Ky]	-2.3		**195** [Prp+Cpx]	-4.4	-4.6				**346** [Ol]	-2.8		**51** [Ol_2]	-7.8	-7.5
5	**91** [Mj]	-2.9	-3.9	**119** [Mj]	-4.1	-4.2	**300** [Prp+Omp]	-4.4	-3.9				**334** [Ol_2]	-7.7	-7.5	**125** [Ol_3]	-3.2	
6	**101** [Mj]	-4.3	-4.1	**127** [Mj]	-3.6	-4.8	**314** [Prp+Omp]	-4.7	-4.8				**227** [En]	-7.4		**271** [Ol+Prp+ En]	-4.8	
7	**132** [Mj]	-3.4	-4.2	**150** [Mj]	-4.7	-6.1	**68** [Prp+Omp]	-4.4	-4.1				**276** [En]	-4.6	-5.1	**41** [Ol]	-1.3	-3.8
8	**249** [Mj]	-3.0	-5.3				**144** [Omp^{min}]	-4.8	-4.5							**137** [En+Co]	-2.1	-4.0
9	**310** [Mj]	-4.0	-4.5 / -4.9				**327** [Omp^{max}]	-4.7	-3.9							**318** [En+Cpx]	-5.5	
10																**149** [Spl]	-6.4	-6.6

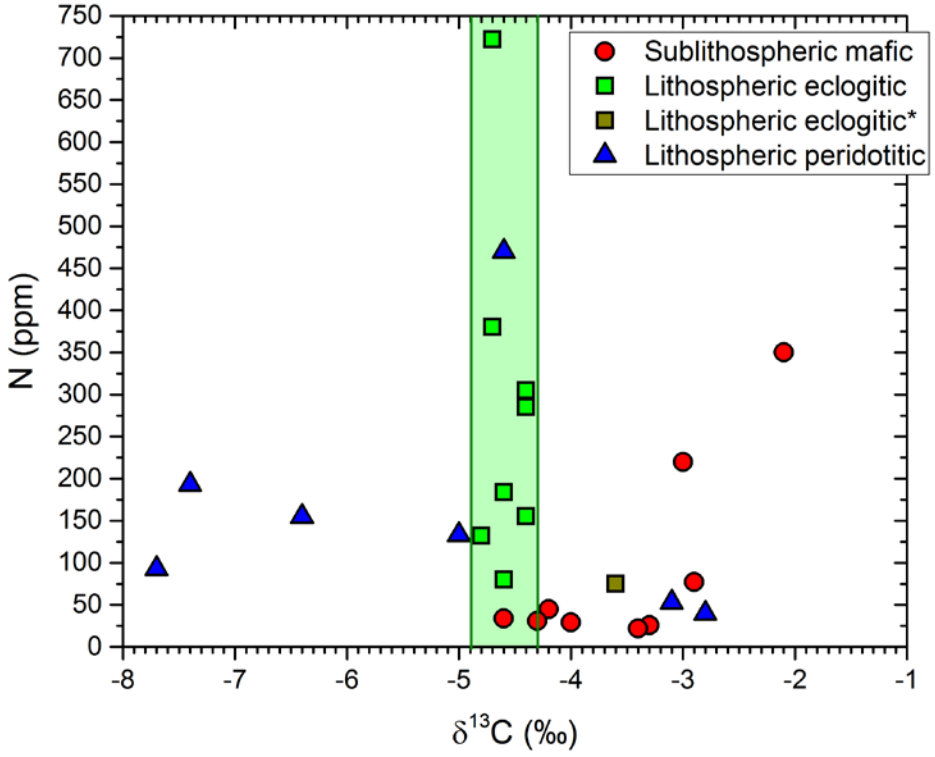

Fig. 8. Carbon isotope composition ($\delta^{13}C$) vs. nitrogen contents (ppm) for type-I Cullinan diamonds with different type of parageneses. Green field points out the narrow $\delta^{13}C$ range for diamonds with eclogitic inclusions.

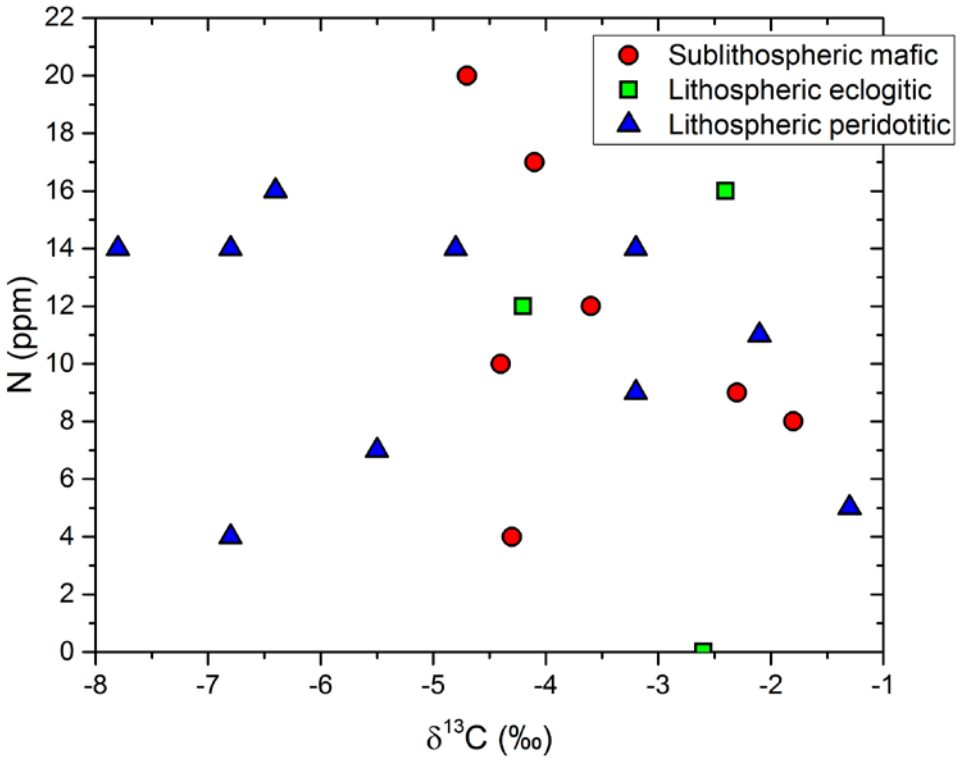

Fig. 9. Carbon isotope composition ($\delta^{13}C$) vs. nitrogen contents (ppm) for type-II Cullinan diamonds with different type of parageneses.

7. Inclusions in diamonds

Three hundred diamonds were polished and two hundred and two diamonds were found to contain 332 silicates and 14 undetermined sulphide phases including 71 minerals from 42 type-II diamonds (ESM 2). The inclusions are diverse (Table 6). Chemical composition of inclusions is given in Electronic Supplementary Material (ESM 3). All inclusions can be divided into four parageneses: lithospheric peridotitic (1) and eclogitic (2), sublithospheric mafic (3) and undetermined, represented by Fe and Fe-Ni sulphides (4). Forty six per cent of Type II diamonds are lithospheric peridotitic containing Cr-pyrope, forsterite, enstatite, clinopyroxene and Cr-spinel. Lithospheric eclogitic stones containing garnet, omphacite, kyanite and coesite comprise 45% of Type II stones, while sublithospheric mafic stones (with Cr-free majorite and CaSiO3) amount to 22%. Lithospheric eclogitic inclusions (Cr-free garnet, omphacite, coesite) appreciably predominate (79%) in the Type I diamonds. Lithospheric peridotitic paragenesis (olivine or enstatite) is minor (14%). Crystals of the sublithospheric mafic association containing Cr-free majorite and CaSiO3 with the perovskite crystal structure as determined by Raman spectroscopy comprise 6% of Type I diamonds. It is possible that some of olivine inclusions from the lithospheric peridotitc association may have originally been wadsleyite or ringwoodite. This would be compatible with the abnormally high temperatures calculated for these olivines using the Al-In-Olivine thermometry (see section on Olivine). This increases the proportion of sublithospheric stones among Type II and Type I diamonds to 33 and 9%.

Table 6. Primary inclusions and mineral parageneses from the studied Cullinan mine diamonds.

Parageneses	Mineral association	Type-I (n diamonds)	Type-II (n diamonds)
Sublithospheric mafic	Mj	5	5
	Mj + Omp	2	1
	Mj + Co + Ky		1
	Mj + Prp-Alm	1	
	$CaSiO_3$ (Wo and Prv)	2	2
Total:		**10** (6%)	**9** (22%)
Lithospheric eclogitic	Grt + Cpx	14	
	Grt ± [Co]	32 [1]	
	Cpx ± [Co]	70	7 [2]
	Co ± [Co]	10	6 [1]
	* En + Co		1
Total:		**126** (79%)	**14** (33%)
Lithospheric peridotitic	Grt + Fo ± [En]	2	2 [1]
	Cr-Aug ± [En]		3 [1]
	Fo	17	13
	En	4	
	Spl		1
Total:		**23** (15%)	**19** (45%)
Lithospheric mixed	Fo + Co	**1** (1%)	
Total:		**160**	**42**

Garnets (non majoritic)

Garnet inclusions are the third most abundant inclusions from the studied Cullinan mine diamonds and they reach the biggest size up to 0.5 mm (Fig. 10). Two non majoritic garnets were found in type-II diamonds and they are high-chromium pyropes with Cr_2O_3 contents about 6.3 and 9.6 wt.%. Garnets from the type-I are extremely diverse. As can be seen in the ternary diagram (Fig. 11) points of garnet from the type-I diamonds lie in the all fields Prp+Knrr, Alm and Grs+Adr+Uv+Sch, but most often garnet belongs to the pyrope-almandine series with very low Cr_2O_3 contents typical of the eclogitic paragenesis (Fig. 12). Also, two high-chromium pyropes (3% of all type-I diamonds with garnet) with Cr_2O_3 contents about 8.8 and 9.1 wt.% were found. Thus, the overwhelming majority of garnet from type-I diamonds are related to the eclogitic paragenesis and, judging by the significant variations of CaO (from 3.2 to 17.0 wt.%), as well as MgO (from 7.4 to 20.1 wt.%) and FeO (from 6.3 to 19.4 wt.%), these garnets are sourced from different types of mantle eclogites. Only four garnets compositions lie in the peridotitic field (Fig. 12). None of the analyzed inclusion grains are zoned.

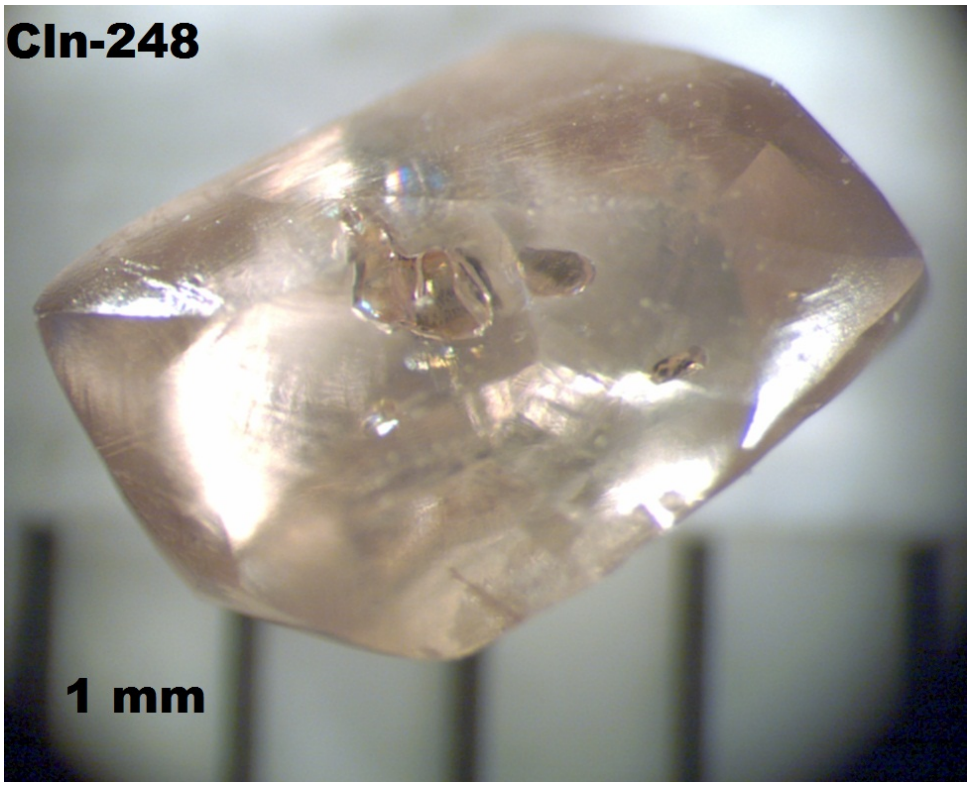

Fig. 10. Large inclusions of garnet (the biggest inclusion Prp49.6 Alm39.0 Grs10.5) in the type-I diamond Cln-248.

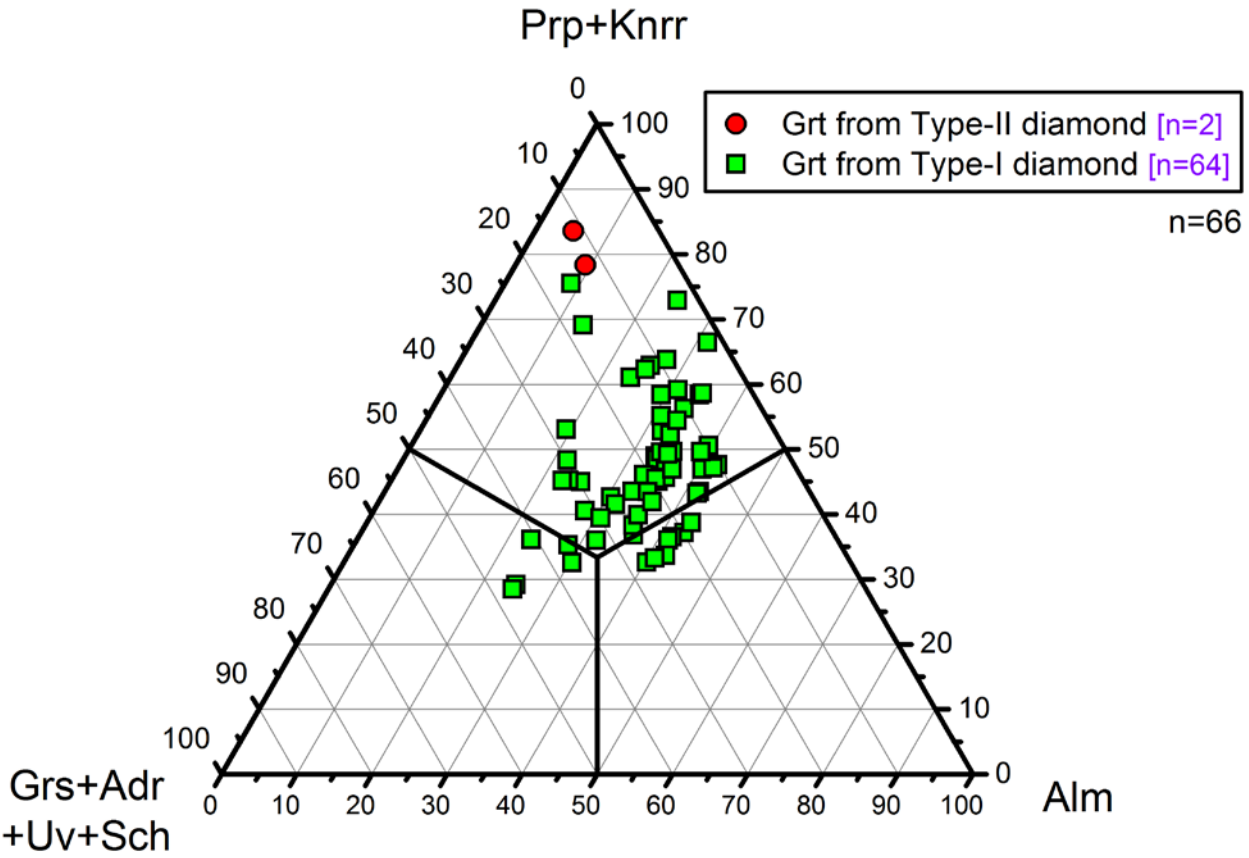

Fig. 11. Ternary diagram showing end-member composition of the garnet inclusions from the studied Cullinan mine diamond. The sum of all mentioned end-members range from 99.2 to 100%. End-members: Pyrope $Mg_3Al_2[SiO_4]_3$ + Knorringite $Mg_3Cr_2[SiO_4]_3$; Almandine $Fe^{2+}{}_3Al_2[SiO_4]_3$; Grossular $Ca_3Al_2[SiO_4]_3$ + Andradite $Ca_3Fe^{3+}{}_2[SiO_4]_3$ + Uvarovite $Ca_3Cr_2[SiO_4]_3$ + Schorlomite $Ca_3Ti_2[(Si,Fe^{3+})O_4]_3$. End-members are calculated according to the method proposed by (Arai, 2010).

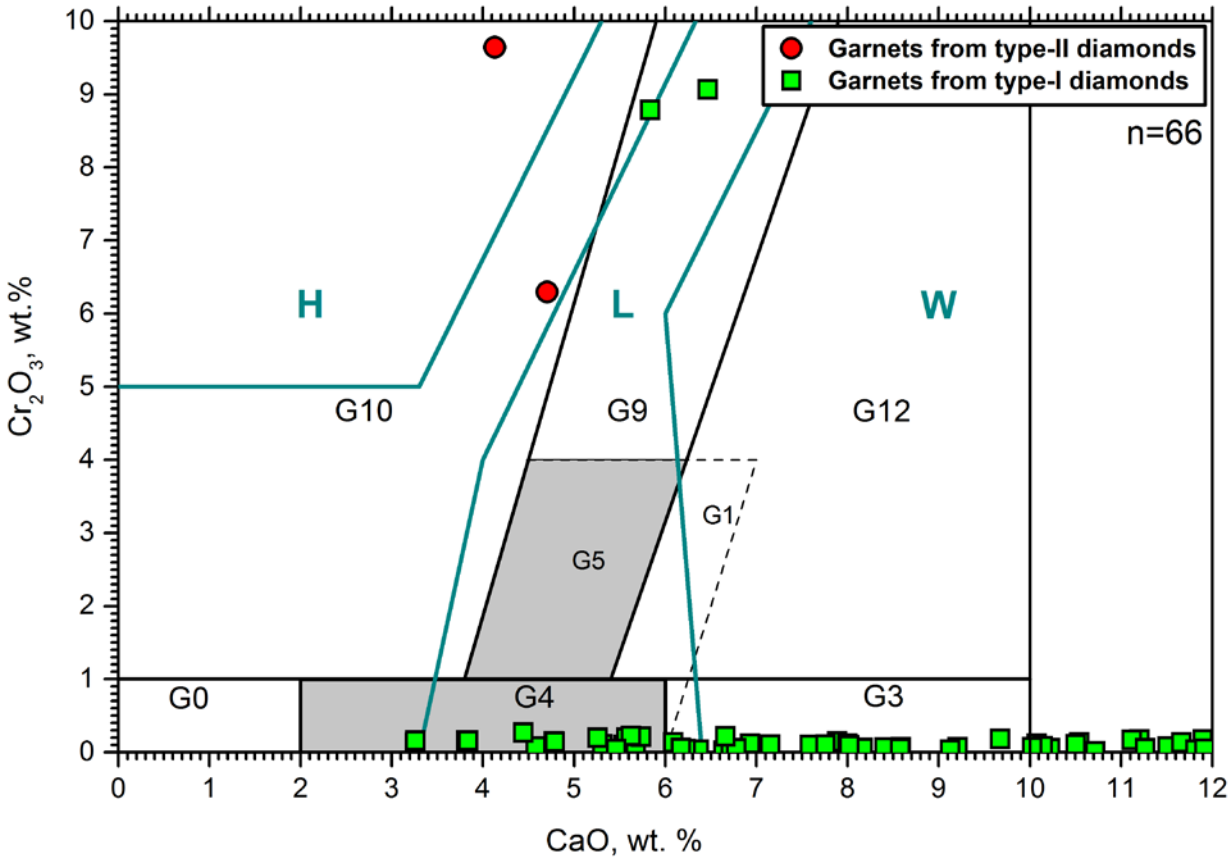

Fig. 12. Garnet composition plotted as Cr_2O_3 vs. CaO. Light blue lines between harzburgitic (H), lherzolitic (L) and all non-peridotitic garnet (Gurney and Zweistra, 1995), and boundary between lherzolitic (L) and wehrlitic field (W) (Sobolev et al., 1973). Black lines and fields G0-G12 from the paper (Grutter et al., 2004).

Clinopyroxene

Clinopyroxene is the most abundant inclusion phase (144 inclusions from 97 diamonds). The composition of clinopyroxene inclusions fluctuates significantly and can be classified as **a)** omphacite, n=109 (Jd from 14 to 30.2 % in cpx from type-II diamonds; Jd from 17.6 to 59,2 in cpx from type-I diamonds), **b)** augite, n=29 (± chromian, ± aluminian, ± sodian, ± ferrian) and **c)** diopside, n=6 (± ferrian, ± aluminian, ±sodian) (Fig. 13-15, ESM 3). Clinopyroxenes from type-I and type-II diamonds are different. Magnesian clinopyroxenes occur in type-II diamonds more frequently, clinopyroxenes from type-II diamonds have Mg# 72.5-92.1, 8 out of 14 have Mg# > 84 and clinopyroxenes from type-I diamonds have Mg# 69.9-90.5 (Fig. 16). Chromian augite (Cr_2O_3 contents 0.8-1.7 wt.%) was found only in type-II diamonds, 4 out of 14 inclusions. In addition, six omphacite inclusions were studied from type-II diamonds, whereas in type-I diamonds omphacites predominate over other types of clinopyroxene (103 out of 130, 79%). The

'A-B-C' classification (Taylor, Neal, 1989) was applied to clinopyroxenes (Fig. 17). Most of inclusions are related to the B-type eclogites, some inclusions originating from A-type eclogites and four inclusions from one type-I diamond can be connected with a C-type eclogite (Ky-eclogite). Some EPMA analyses of clinopyroxenes have oxide totals around 96-97 wt.%, probably related to partial secondary alteration to hydrous minerals.

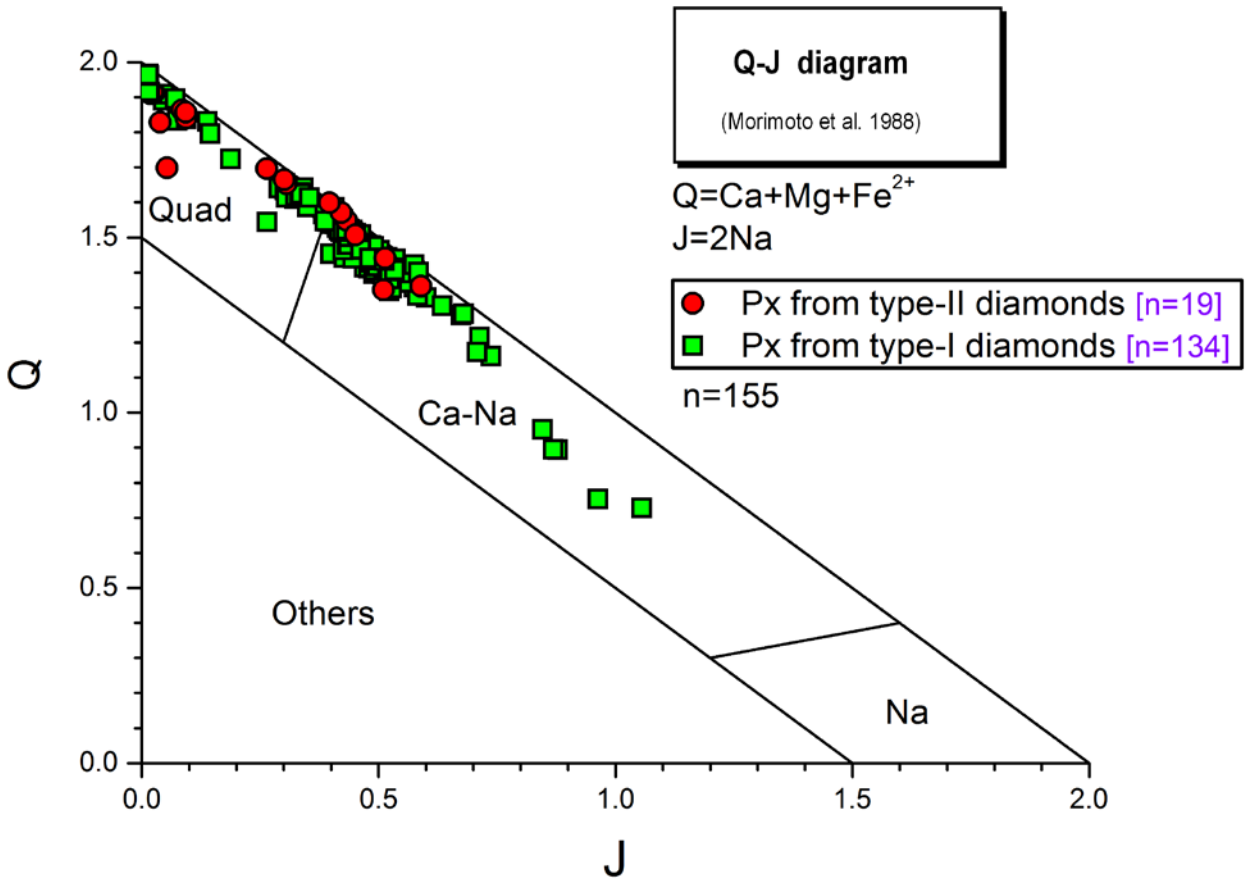

Fig. 13. Q-J diagram (Morimoto et al., 1988), where Q=Ca+Mg+Fe^{2+} (apfu) and J=2*Na (apfu) for the pyroxene from the studied Cullinan mine diamonds.

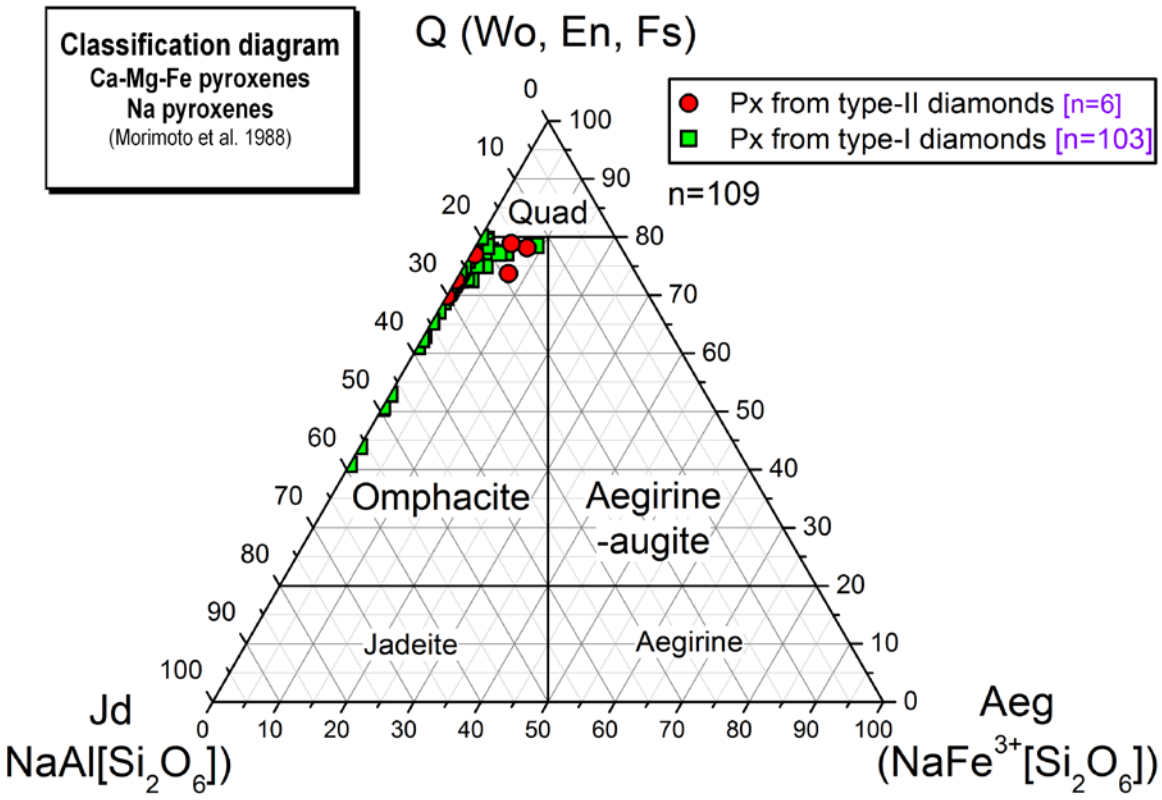

Fig. 14. Pyroxenes from the studied Cullinan mine diamond on the classification diagrams for Ca-Na pyroxenes (Morimoto et al., 1988).

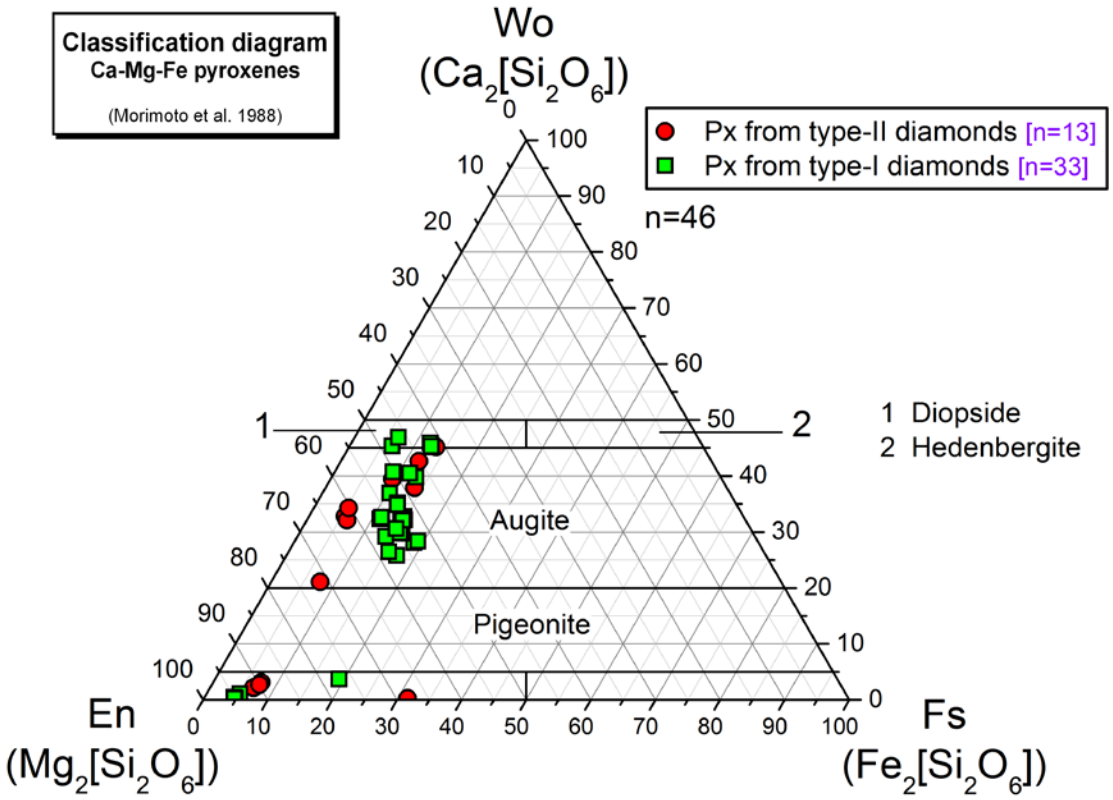

Fig. 15. Pyroxenes from the studied Cullinan mine diamond on the classification diagrams for Ca-Fe-Mg pyroxenes (Morimoto et al., 1988).

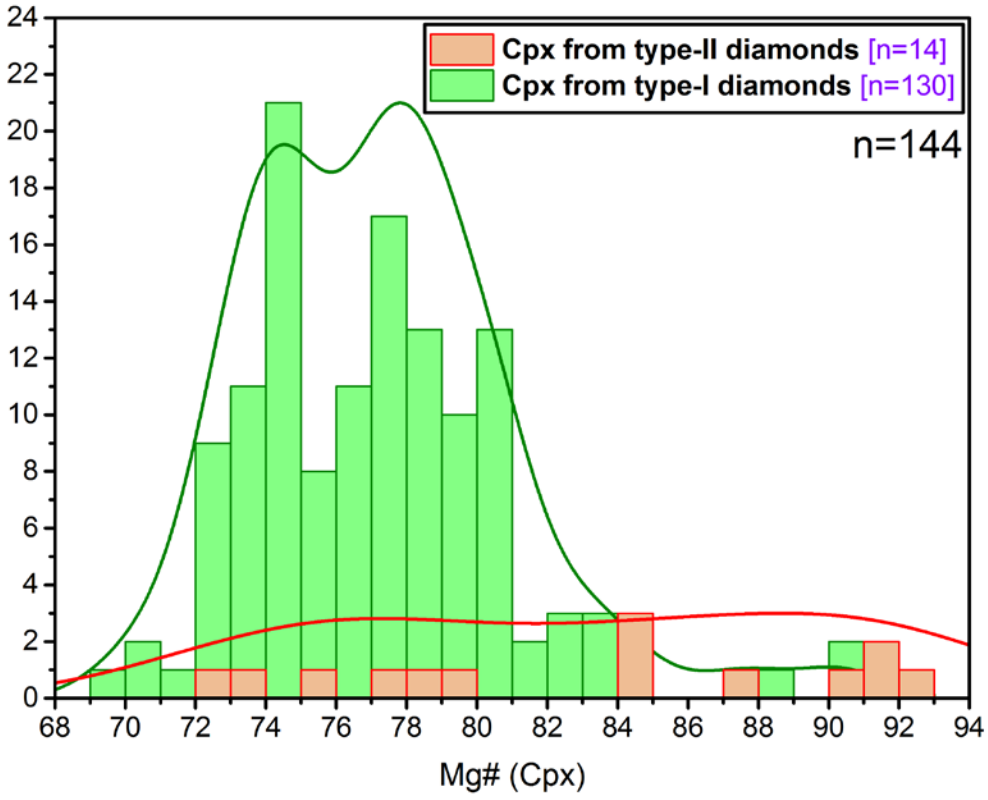

Fig. 16. Distribution of the clinopyroxene Mg# of the studied Cullinan mine diamonds. Lines are distribution curves (kernel smoothed).

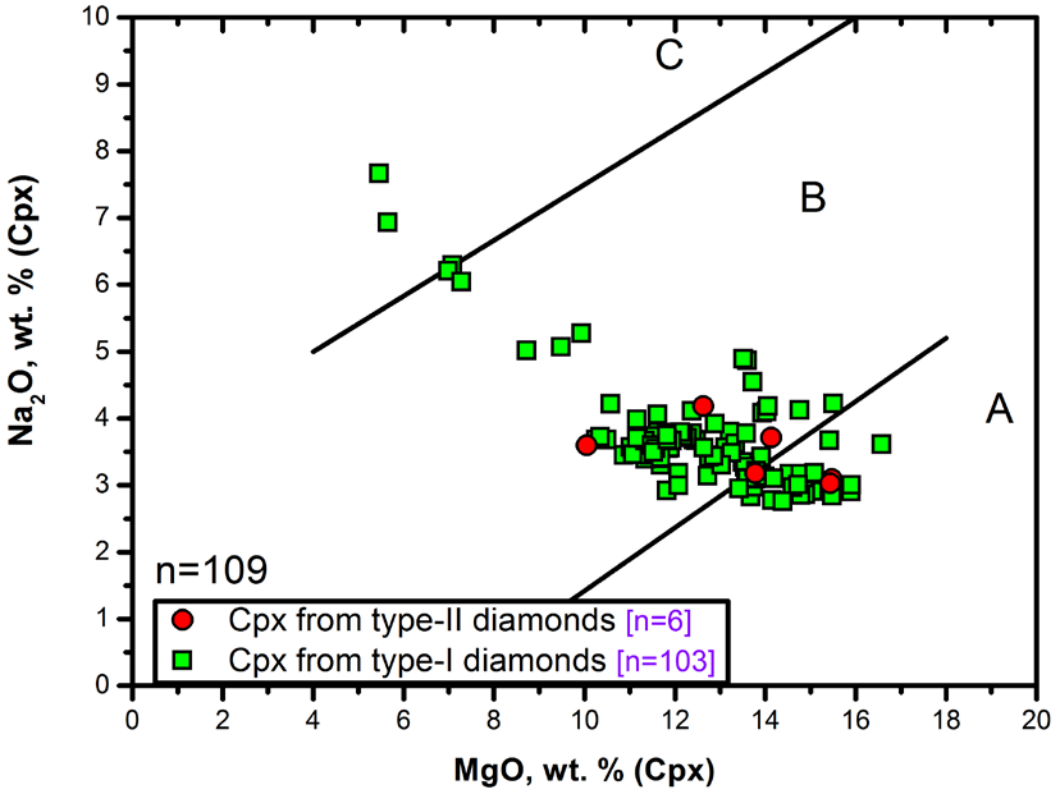

Fig. 17. Clinopyroxenes from the studied Cullinan mine diamond on the A-B-C classification scheme (Taylor, Neal, 1989).

Orthopyroxene

All orthopyroxene inclusions (n=11) are represented by enstatite (Fig. 15). The chemical compositions of the nine inclusions are very similar. Al_2O_3 concentration is not more than 1.0 wt.%. Enstatitie end-member ranges from 89 to 95%. (ESM 3) According to the conclusions of (Boyd et al., 1997) it may indicate that they are associated with garnet peridotite. If the Al_2O_3 exceeds about 1.5 wt.% or more, it would result from inversion of the original high-pressure Mg-Si-perovskite crystal lattice of MgSiO3 or from an origin in spinel peridotite. Chemical composition of enstatites from samples Cln-137 and Cln-276 is very different from the other enstatites. These two samples contain more Al_2O_3 (9.6 and 1.7 wt.%, accordingly), less MgO (enstatitie end-member is about 68 and 77%, accordingly) and about 0 wt.% of Cr_2O_3. It may indicate that they are associated with eclogite or websterite.

Olivine

Olivine is one of the most common inclusions. All studied olivines are forsterites. Differences in the chemical composition of the olivines from type-I and type-II diamonds have not been identified. Mg# (100* molar Mg/(Mg+Fe)) of olivine inclusions (n=42) ranges from 90.0 to 95.3 with a mean of 92.3, excepting one inclusion from Cln-41 diamond with 75.2 of Mg#. According to the worldwide dataset compiled in (Stachel and Harris, 2008), the overwhelming majority of olivines are sourced from lherzolite (average #Mg 92.0), rather than harzburgite (average #Mg 93.2). Furthermore, contents of trace elements in the 17 largest olivine inclusions were analyzed by LA-ICP-MS (Electronic Supplementary Material, ESM 4). It should be noted that the high vanadium concentrations are observed in some olivine inclusions in comparison with olivines from different types of mantle xenoliths and all olivine inclusions fall along the garnet-facies trend (Fig. 18).

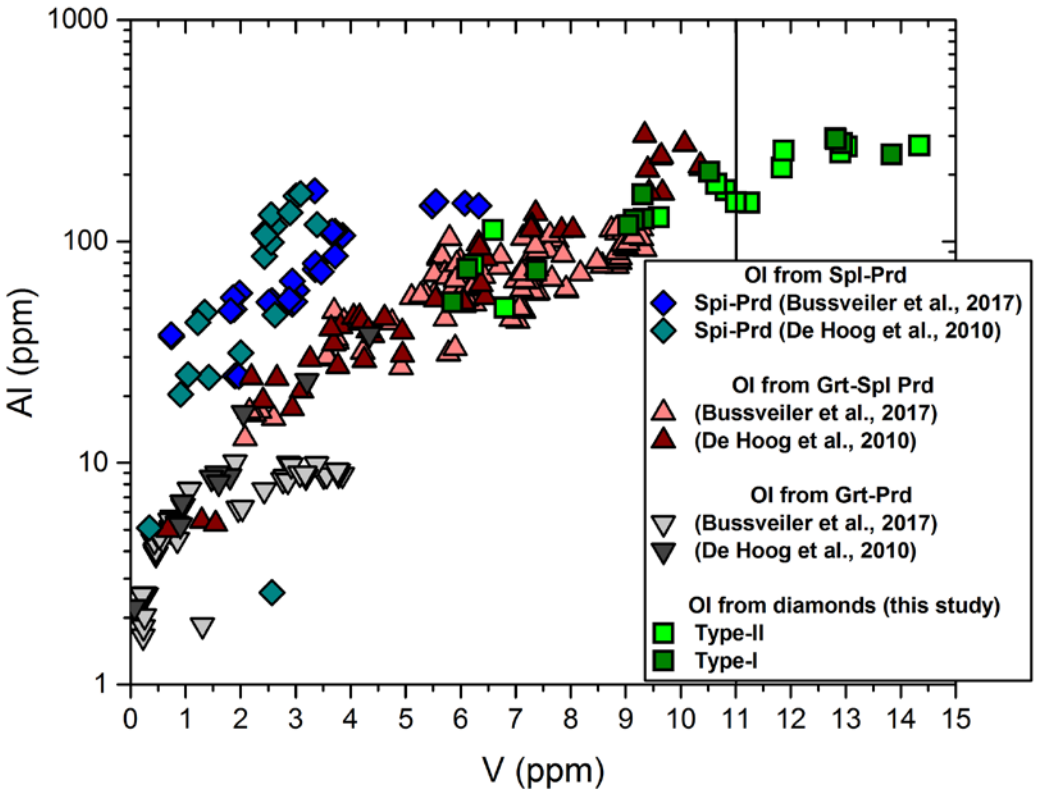

Fig. 18. Al versus V concentration in olivines from different xenolith facies based on data from De Hoog et al., (2010); Bussweiler et al., (2017) and in the olivine inclusions from the studied Cullinan mine diamond (this study).

CaSiO3 (Ca-Perovskite and wollastonite)

Only three 3 CaSiO3 inclusions were found. Two inclusions from type-II diamonds as shown by Raman spectroscopy have the wollastonite crystal lattice. The chemical compositions of all phases are similar. However, one inclusion with the Ca-Si-perovskite crystal structure was found in a type-I diamond (Fig. 19). This is the first finding of an unreverted Ca-Si-perovskite. The most intense Raman peaks for uninverted Ca-Si-perovskite are the following (in order of decreasing intensity and in cm^{-1}): 778, 246, 337, 470, 224, 285, 436, 397, 380 and 494 (Fig. 19). X-ray single-crystal study confirmed that founded mineral phase has perovskite crystal structure, with follow crystallographic parameters:

Crystal system: *Orthorhombic*

Space group: *Pbnm*

Cell parameters:
a 5.397 (4) Å
b 5.404 (4) Å
c 7.646 (4) Å
V 223.0 (3) Å3
Z = 4

All collected information about described inclusion was processed and submitted as a new mineral application to the Commission on new minerals, nomenclature and classification of the International Mineralogical Association.

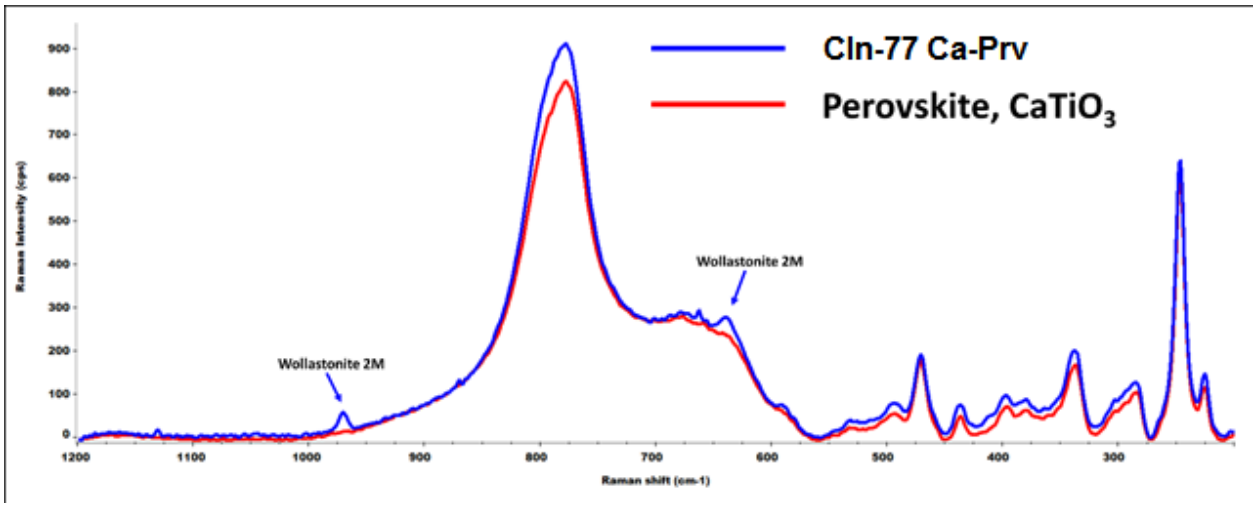

Fig. 19. Raman spectrum of CaSiO3 inclusion from the type-I diamond (Cln-77, blue line) in comparison to the spectrum of the standard perovskite (RRUFF Raman database, red line). The two spectra are almost identical with the only difference definitively marked by a few

Raman peaks likely belonging to wollastonite 2M (RRUFF Raman database, La Fuente et al. 2015).

Majorite

Seventeen majorite inclusions were found in 14 diamonds (6 in type-II and 11 in type-I diamonds). All majorities contain very low Cr_2O_3 concentration (up to 0.25 wt.%), indicating connection with mantle eclogites. Si (apfu) in the octahedral position is 0.05-0.26; Na (apfu) in the dodecahedral is 0.08-0.18 (ESM 3).

Coesite

Coesite is a common phase in type-II and type-I diamonds (42 inclusions in 22 diamonds, ESM 2). Other eclogitic inclusions (kyanite, omphacite and majorite) were found together with coesite.

Spinel

There are five spinel inclusions in the 4 type-II diamonds. Their chemical composition varies strongly. One diamond (Cln-149) contains two primary inclusions of magnesiochromite (Mg (apfu) 0.75-0.76 and Cr (apfu) 1.66-1.68) which most likely associate with spinel peridotite. Other diamonds contain secondary spinel with the significant hercynite end-member (Fe (apfu) 0.36 and 0.49) (ESM 3).

Kyanite

Two kyanite inclusions were found in the type-II diamonds. In both cases, diamonds also include coesite (ESM 2).

Sulphides

A preliminary study of sulfides is shown that these minerals are represented by Fe and Fe-Ni phases. Two phases have a good correspondence with standard Raman spectra of pyrite and troilite.

Secondary minerals

Secondary minerals are quite diverse and similar to the set of secondary minerals in mantle xenoliths and kimberlites. They can replace primary inclusions (amphibole replace pyroxene; talk replace olivine (Fig. 20)) and are localized in open and sealed cracks. Secondary mineral association is represented by amphibole (actinolite-tremolite series, edenite or hornblende), serpentine, talc, mica (phlogopite, biotite), microcline, apatite and, perhaps, sellaite (MgF_2) which was found in cracks from several diamonds. Representative chemical compositions of some secondary minerals are given in the Electronic Supplementary Materials (ESM 3).

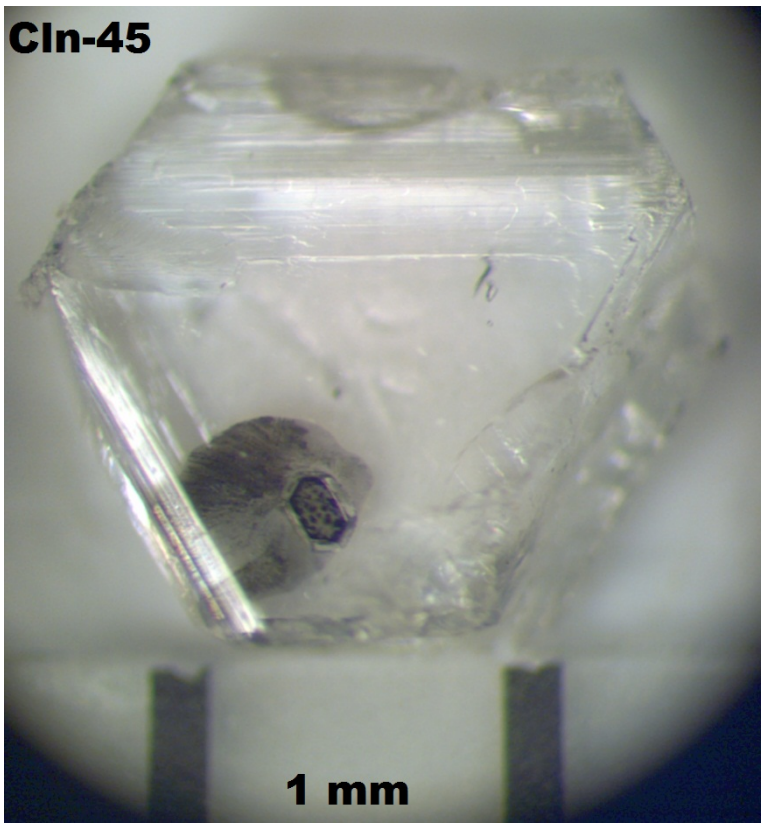

Fig. 20. Large olivine inclusion completely replaced by talk in macle type-II diamond Cln-45.

8. Thermobarometry

The temperatures were evaluated using an Al-in-Ol thermometer (Bussveiler et al., 2017) (Table 7), an Opx-Cpx (Taylor, 1998) thermometer with a Opx-Grt barometer (Nickel, Green, 1985) and a single crystal Cpx (Nimis, Taylor, 2000) thermometer for peridotitic inclusions and a Grt-Cpx thermometer (Nakamura, 2009) for eclogitic inclusions (Table 8). The temperatures are projected on the local geotherm constrained by the Cullinan peridotitic xenoliths (Viljoen et al., 2009) and approximated by a 40 mW/m^2 geotherm (Hasterok and Chapman, 2011; Furlong and Chapman, 2013). To calculate the pressure of majorities, the new improved majorite geobarometer was chosen (Wijbrans et al., 2016). More than two thirds of the inclusions show PT-parameters consistent with the lithospheric conductive thermal regime, 1090-1400°C and 45-63 kb. We did not find any correlations between the diamond type and the temperatures of formation for lithospheric diamonds. Less than one third of the inclusions yields temperatures higher than the upper error limit of the upper mantle adiabat (Katsura et al., 2010) shown as a gray area on the PT-diagram of Fig. 21. The majorite barometry yields pressures of 93-138 kb (17 samples) when projected onto 1327 and 1440°C adiabats. The sublithospheric mafic diamonds are thus sourced from the transition zone, based on the stability of Ca-Si perovskite (below 500 km) and the 370-445 km inferred depth of majorite origin. For the lithospheric diamonds, the PT-conditions of origin for inclusions of eclogitic and peridotitic parageneses are identical (Fig. 21).

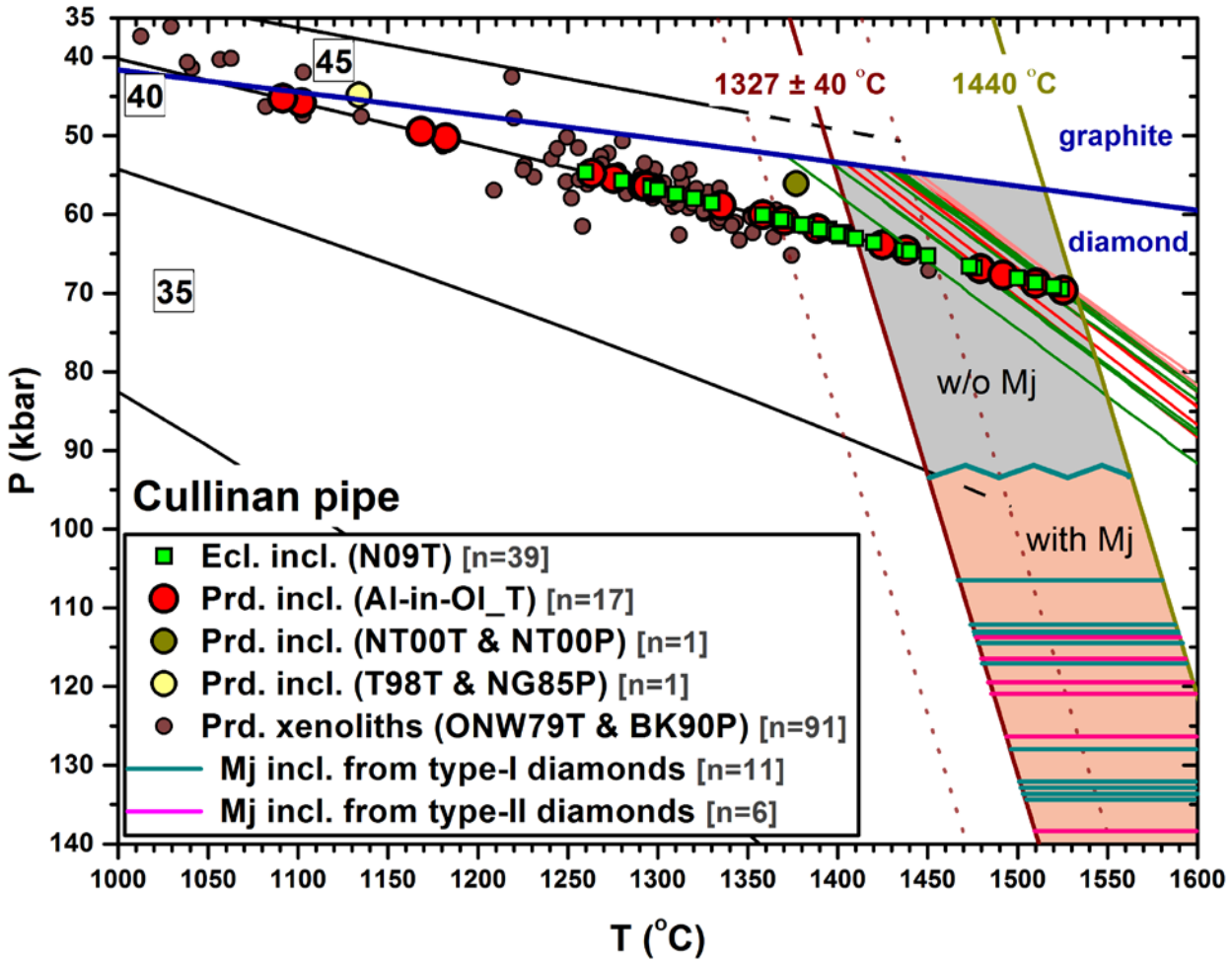

Fig. 21. Pressure-temperature estimates for studied Cullinan diamond inclusions and inclusion in diamonds from different localities using the following thermometers and barometers: Eclogite association, (N09T) – garnet-clinopyroxene thermometer (Nakamura, 2009); Peridotite association, (Al-in-Ol_T) - Al-in-olivine thermometer (Bussweiler et al., 2017); (NT00T & NT00P) - Single-clinopyroxene geothermobarometer (Nimis, Taylor, 2000); (T98T & NG85P) - Orthopyroxene-clinopyroxene thermometer (Taylor, 1998) and orthopyroxene-garnet barometer (Nickel, Green, 1985) and (ONW79T & BK90P) - Olivine-garnet thermometer (O'Neill and Wood, 1979) and Al-in-orthopyroxene barometer (Brey et al., 1990); Sublithospheric mafic association, Mj geobarometer (Wijbrans et al., 2016). The temperatures obtained by means of (N09T) and (Al-in-O_Tl) thermometers are projected on the local geotherm constrained by the Cullinan peridotitic xenoliths (Viljoen et al., 2009) and approximated by a 40 mW/m^2 geotherm (Hasterok and Chapman, 2011; Furlong and Chapman, 2013). Model conductive geotherms labeled 35, 40 and 45 are after (Hasterok and Chapman, 2011; Furlong and Chapman, 2013); they terminate at a mantle adiabat with the surface temperature 1327 ± 40°C and the temperature gradient 0.4°C/km (Katsura et al., 2010). Graphite-diamond phase boundary of Day (2012) is shown by the blue line. The green and red univariant P-T lines calculated from Grt-Cpx (Nakamura, 2009) and Al-in-Ol (Bussweiler et al., 2017) thermometers for eclogitic and peridotitic inclusions accordingly. The 1440°C potential temperature found from an intersection of the univariant P-T lines for eclogitic and peridotitic inclusions with the highest PT-parameters with the local geotherm. Dark field is a probable area of origin for eclogitic diamonds with high Cpx-Gar temperatures and peridotitic diamonds with

high Al-in-Ol temperatures. The field is limited by the ambient 1327°C adiabat, the 1440°C adiabat, the 40 mW/m2 geotherm (Hasterok and Chapman, 2011) and majoritic inclusion with the lowest PT-parameters.

Table 7. Aluminum contents and PT-parameters of olivine inclusions (lithospheric peridotitic paragenesis) from Cullinan diamonds. Al-in-Ol_T & 40G_P - Al-in-olivine thermometer (Bussweiler et al., 2017) in combination with the 40 mW/m^2 model conductive geotherm (Hasterok and Chapman, 2011; Furlong and Chapman, 2013); Al-in-Ol_T & IHN99P - Al-in-olivine thermometer (Bussweiler et al., 2017) in combination with the olivine Raman barometer (Izraeli et al., 1999); Al-in-Ol_T & K14P - Al-in-olivine thermometer (Bussweiler et al., 2017) in combination with the olivine Raman barometer (Kohn, 2014).

Type of diamond	**Sample**	**Al^{Ol} (ppm)**	**T (°C)**	**P (kbar)**	**T (°C)**	**P (kbar)**	**T (°C)**	**P (kbar)**
			Al-in-Ol_T & 40G_P		**Al-in-Ol_T & IHN99P**		**Al-in-Ol_T & K14P**	
I	Cln-33	53.1	1100	46	-	-	-	-
		126.6	1275	55				
I	Cln-34	125.1	1290	56	-	-	-	-
		118.2	1290	56				
I	Cln-281	163.4	1340	59	1420	75	1345	61
I	Cln-294_1	75.1	1170	49	-	-	-	-
I	Cln-294_2	73.8	1170	49	-	-	-	-
I	Cln-328	246.7	1480	67	1476	66	1453	62
I	Cln-334	278	1520	69	1491	63	1495	64
		289.6	1530	70				
I	Cln-346	205.9	1420	64	-	-	-	-
II	Cln-6	271.4	1510	69	1471	62	1477	63
II	Cln-17	112.4	1260	55	-	-	-	-
II	Cln-42	215.4	1440	64	1441	65	1417	61
II	Cln-51	170.1	1370	61	1382	63	1357	58
		182.2	1390	62				
II	Cln-53	256.3	1490	68	1486	67	1464	63
		268.4	1490	67				
II	Cln-125	252.1	1510	69	1500	67	1477	63
		291.6	1530	70				
II	Cln-233	50.3	1090	46	1143	56	1109	49
II	Cln-271	149.5	1360	60	-	-	-	-
		150.0	1360	60				
II	Cln-335	128.4	1300	56	1295	57	1288	55
II	Cln-341	78.5	1180	50	1201	54	1185	51

Table 8. PT-parameters of garnet-clinopyroxene inclusions (lithospheric eclogitic paragenesis) from Cullinan diamonds. Pressure-temperature estimates for inclusion from Cullinan diamonds using Grt-Cpx thermometer (Nakamura, 2009) in combination with the 40 mW/m^2 geotherm (Hasterok and Chapman, 2011; Furlong and Chapman, 2013).

N	Sample	Ecl. Type	Accociation	T (°C)	P (kbar)
1	Cln-68	B	Omp_1 / Grt_1	1470	67
		B	Omp_1 / Grt_2	1480	67
		B	Omp_1 / Grt_3	1380	61
		B	Omp_1 / Grt_4	1380	61
2	Cln-106	B	Omp_1 / Grt_1	1390	62
		B	Omp_2 / Grt_1	1400	62
3	Cln-110	B		1390	62
4	Cln-139	B		1400	63
5	Cln-145	Grsp	Di_1 / Grt_1	1300	57
		Grsp	Di_2 / Grt_1	1290	56
6	Cln-164	B		1470	67
7	Cln-176	B		1370	61
8	Cln-195	A	Omp_1 / Grt_1	1550	71
		A	Omp_2 / Grt_1	1570	72
		A	Omp_1 / Grt_2	1510	69
		A	Omp_2 / Grt_2	1530	70
9	Cln-300	B	Omp_1 / Grt_1	1280	56
		B	Omp_1 / Grt_2	1320	58
10	Cln-306	B	Omp_1 / Grt_1	1350	60
		B	Omp_1 / Grt_2	1360	60
11	Cln-308	B		1440	65
12	Cln-314	B	Omp_1 / Grt_1	1380	61
		B	Omp_2 / Grt_1	1360	60
13	Cln-324	B		1400	63
14	Cln-355	B		1400	63

Studied diamonds from Cullinan pipe contain more inclusion with superadiabatic PT-parameters than other kimbrlite pipes. Peridotitic inclusions with superadiabatic PT-parameters are more than 40% (n=17, 41.2%, this study, table 7) and eclogitic inclusions with superadiabatic PT-parameters are not less than 50% (n=37, 54.1%; 14 samples in this study, table 8; 1 sample from Tsai et al., 1979; 21 sample from Gurney et al., 1985; 1 sample from Viljoen et al., 2010) out of all inclusions from Cullinan diamonds. Previously studied Premier diamonds show P-Ts higher than other Kaapvaal diamonds, but not super-adiabatic, not as high as the collection we investigated.

9. Conclusions and results

1. Studied Cullinan diamonds conatain inclusions of four parageneses: lithospheric peridotitic (1) and eclogitic (2), sublithospheric mafic (3) and undetermined, represented by Fe and Fe-Ni sulphides (4).

2. Lithospheric peridotitic paragenesis predominates in Type II diamonds, whereas 79% Type I stones are sourced from eclogites. The result confirms a well-known fact that E-type diamonds contain more nitrogen than P-type diamonds. Nevertheless, there is no strict correlation between the type of diamond and the paragenesis.

3. The overwhelming majority of lithospheric peridotitic inclusions originated from a mantle lherzolite, as evidenced by the chemical composition of garnets (Fig. 12), the average Mg# of olivines (92.3), which is very close to the lherzolitic olivine diamond inclusions of the worldwide dataset (92.0) (Stachel, Harris, 2008) and the low Al_2O_3 contents in enstatites (below 1.0 wt.%; Boyd et al., 1997). The lithospheric eclogitic inclusions are very diverse, with ranges of garnet composition Prp 28.3-72.8, Alm 19.3-43.2, Grs 1.6-46.1 (Fig. 11 and 12) and ranges of omphacite composition Jd 12.5-59.2, Aeg 0-9.0, Wo+En+Fs 40.8-80.0 (Fig. 14). These facts suggest that the studied minerals represented all A, B and C types of eclogite (Fig.17) (Taylor, Neal, 1989). Moreover, one type-I diamond (cln-145) contains grossular and diopside inclusions similar to the grospiditic association.

4. The distribution of paragenesis in type-I and -II diamonds may reflect a natural N heterogeneity of the parent diamondiferous rocks, but may also be controlled by the external diamond-forming fluid.

5. Another contrast between Type II and Type I stones is the higher abundance of sublithospheric inclusions in the former, indicating the more common derivation from the transition zone, where low N contents in Cullinan sublithospheric diamonds may be linked to the presence of Fe or FeC (Smith et al., 2014; 2016). We conclude that type II diamonds are diverse in the paragenesis and consequently in the origin.

6. Studied diamonds from Cullinan pipe contain more inclusion with superadiabatic PT-parameters than diamonds from other kimbrlite pipes. Extra high P-Ts of inclusions, mineral set with ultradeep phases (majorite, Ca-Prv with wollastonite and perovskite crystal structure), age of some inclusions (1930±60 Ma, Sm-Nd isotope system, P-type gnt+cpx Lhz inclusions (Richardson et al., 1993)) close to emplacement age of Bushveld complex (2055-2060 Ma (Kruger 1989; Harmer and Armstrong, 2000; de Waal et al., 2001; Mapeo et al., 2004)) and comparison with mantle xenolits from Cullinan kimberlites suggest that origin of Cullinan diamond could be associated with plume activity.

10. Publications and results dissemination

A result of current study was submitted to the 11th International Kimberlite Conference (11 IKC). The Kimberlite Conference is the most influential conference in the world on the subject of diamond geology, diamond origin and diamond mining. The Long Abstract is attached (ESM 5). Oral presentation is scheduled for September 20, 2017. Oral technical Programme is attached (ESM 6). All collected information about CaSiO3 inclusion with perovskite crystal structure was processed and submitted as a new mineral application to the Commission on new minerals, nomenclature and classification of the International Mineralogical Association. It is expected that the decision will be known at the beginning of August.

In addition, I am planning to submit the result of the project to the following journals:

1) "Discovery of high pressure CaSiO3-pervoskite in diamond confirms the major host for Ca in Earth's lower mantle" by F. Nestola, N. Korolev, M. Kopylova, N. Rotiroti, D.G. Pearson, M.G. Pamato, M. Alvaro, J.J. Gurney, A.E. Moore, J. Davidson, will be submitted to NATURE.

2) "The origin of Type II diamonds: Insights from contrasting mineral inclusions in Cullinan Type I and Type II stones" by N. Korolev, M. Kopylova, Y. Bussweiler, D.G. Pearson, J. Gurney, A.E. Moore, J. Davidson, will be submitted to Mineralogy and Petrology.

3) "Plume-generated diamonds: The uniquely high-temperature character of Premier diamonds", N. Korolev, M. Kopylova, Y. Bussweiler, D.G. Pearson, J. Gurney, A.E. Moore, J. Davidson, will be submitted to Earth and Planetary Science Letters.

References

Arai, H. (2010). A function for the R programming language to recast garnet analyses into end-members: Revision and porting of Muhling and Griffin's method// Computers & Geosciences, 36(3), 406-409.

Boyd, F.R., Pokhilenko, N.P., Pearson, D.G., Mertzman, S.A., Sobolev, N.V., Finger, L.W. (1997). Composition of the Siberian cratonic mantle: evidence from Udachnaya peridotite xenoliths// Contributions to Mineralogy and Petrology, 128(2-3), 228-246.

Brey, G.P., Köhler, T. (1990). Geothermobarometry in four-phase lherzolites II. New thermobarometers, and practical assessment of existing thermobarometers// Journal of Petrology, 31(6), 1353-1378.

Bussweiler, Y., Brey, G.P., Pearson, D.G., Stachel, T., Stern, R.A., Hardman, M.F., Kjarsgaard, B.A., Jackson, S.E. (2017). The Aluminum-in-Olivine Thermometer for Mantle Peridotites-Experimental versus Empirical Calibration and Potential Applications// Lithos, 272-273, 301-314.

Day, H.W. (2012). A revised diamond-graphite transition curve// American Mineralogist, 97, 52-62.

De Hoog, J.C., Gall, L., Cornell, D.H. (2010). Trace-element geochemistry of mantle olivine and application to mantle petrogenesis and geothermobarometry// Chemical Geology, 270(1), 196-215.

Deines, P., Gurney, J.J., Harris, J.W. (1984). Associated chemical and carbon isotopic composition variations in diamonds from Finsch and Premier kimberlite, South Africa// Geochimica et Cosmochimica Acta, 48, 325-342.

Deines, P., Harris, J.W., Spear P.M., Gurney, J.J. (1989). Nitrogen and ^{13}C content of Finsch and Premier diamonds and their implications// Geochimica et Cosmochimica Acta, 53, 1367-1378.

Deines, P., Harris, J.W. (1995). Sulfide inclusion chemistry and carbon isotopes of African diamonds// Geochimica et Cosmochimica Acta, 59(15), 3173-3188.

De Waal, S.A., Maier, W.D., Armstrong, R.A., Gauert, Christoph, D.K. (2001). Parental magma and emplacement of the stratiform Uitkomst Complex, South Africa// Canadian Mineralogist, 39(2), 557-571.

Furlong, K.P., Chapman, D.S. (2013). Heat flow, heat generation, and the thermal state of the lithosphere// Annual Review of Earth and Planetary Sciences, 41, 385-410.

Grütter, H.S., Gurney, J.J., Menzies, A.H., Winter, F. (2004). An updated classification scheme for mantle-derived garnet, for use by diamond explorers// Lithos, 77(1), 841-857.

Gurney, J.J., Harris J.W., Rickard R.S., Moore R.O. (1985). Inclusions in Premier mine diamonds// Transactions of the Geological Society of South Africa, 301-310.

Gurney, J.J., Zweistra, P. (1995). The interpretation of the major element compositions of mantle minerals in diamond exploration// Journal of Geochemical Exploration, 53(1-3), 293-309.

Harmer, R.E., Armstrong, R.A. (2000). Duration of Bushveld Complex (sensu lato) magmatism: constraints from new SHRIMP zircon chronology// In workshop on the Bushveld Complex, 18-21.

Hasterok, D., Chapman, D.S. (2011). Heat production and geotherms for the continental lithosphere// Earth and Planetary Science Letters, 307(1), 59-70.

Izraeli, E.S., Harris, J.W., Navon, O. (1999). Raman barometry of diamond formation// Earth and Planetary Science Letters, 173, 351-360.

Katsura, T., Yoneda, A., Yamazaki, D., Yoshino, T., Ito, E. (2010). Adiabatic temperature profile in the mantle// Physics of the Earth and Planetary Interiors, 183(1), 212-218.

Kohn, M.J. (2014). “Thermoba-Raman-try”: Calibration of spectroscopic barometers and thermometers for mineral inclusions// Earth and Planetary Science Letters, 388, 187-196.

Kruger, F. J. 1989. The geochronology and Sr-isotope geochemistry of the Molopo Farms Complex, Bushveld Magmatic Province: a preliminary report. Molopo Botswana (Pty) Ltd. Final Report for Prospecting Licences 14/85 and 38/90. Open File Report, Geological Survey Botwsana.

Kuskov, O.L., Fabrichnaya, O.B. (1990). Phase relationships in the FeO-MgO-SiO2 system at the boundary between the transition zone and the lower mantle// Geochemistry International, 27(9-12), 95.

La Fuente, B., Downs, R.T., Yang, H., Stone, N. (2015) The power of databases: the RRUFF project. In: Highlights in Mineralogical Crystallography, T Armbruster and R M Danisi, eds. Berlin, Germany, W. De Gruyter, pp. 1-30.

Mapeo, R.B.M., Kampuznu, A.B., Ramokate, L.V., Corfu, F., Key, R.M. (2004). Bushveld-age magmatism in southeastern Botswana: evidence from U-Pb zircon and titanite geochronology of the Moshaneng Complex// South African Journal of Geology, 107, 219-232.

Mendelssohn, M.J., Milledge, H.J., 1995. Geologically significant information from routine analysis of the mid-infrared spectra of diamonds// International Geology Review 37, 95–110.

McCallum, M.E., Huntley, P.M., Falk, R.W., Otter, M.L. (1994). Morphological, resorption and etch feature trends of diamonds from kimberlite populations within the Colorado-Wyoming State Line district, USA// In Proceedings of the 5th International Kimberlite Conference (Vol. 2, pp. 32-50).

Morimoto, N. (1988). Nomenclature of pyroxenes// Mineralogy and Petrology, 39(1), 55-76.

Nakamura, D. (2009). A new formulation of garnet–clinopyroxene geothermometer based on accumulation and statistical analysis of a large experimental data set// Journal of Metamorphic Geology, 27(7), 495-508.

Nickel, K.G., Green, D.H. (1985). Empirical geothermobarometry for garnet peridotites and implications for the nature of the lithosphere, kimberlites and diamonds// Earth and Planetary Science Letters, 73(1), 158-170.

Nimis, P., Taylor, W.R. (2000). Single clinopyroxene thermobarometry for garnet peridotites. Part I. Calibration and testing of a Cr-in-Cpx barometer and an enstatite-in-Cpx thermometer// Contributions to Mineralogy and Petrology, 139(5), 541-554.

O'Neill, H. S.C., Wood, B.J. (1979). An experimental study of Fe-Mg partitioning between garnet and olivine and its calibration as a geothermometer// Contributions to Mineralogy and Petrology, 70(1), 59-70.

Paton, C., Hellstrom, J., Paul, B., Woodhead, J., Hergt, J. (2011). Iolite: Freeware for the visualisation and processing of mass spectrometric data// Journal of Analytical Atomic Spectrometry, 26(12), 2508-2518.

Smith, E.M., Kopylova, M.G. (2014). Implications of metallic iron for diamonds and nitrogen in the sublithospheric mantle// Canadian Journal of Earth Sciences, 51,510-516.

Smith, E.M., Shirey, S.B., Nestola, F., Bullock, E.S., Wang, J., Richardson, S.H., Wang, W. (2016). Large gem diamonds from metallic liquid in Earth's deep mantle// Scince, 354(6318), 1403-1405.

Sobolev, N.V., Lavrent'ev, Y.G., Pokhilenko, N.P., & Usova, L.V. (1973). Chrome-rich garnets from the kimberlites of Yakutia and their parageneses// Contributions to Mineralogy and Petrology, 40(1), 39-52.

Stachel, T., Harris, J.W. (2008). The origin of cratonic diamonds – constraints from mineral inclusions. Ore Geology Reviews, 34(1), 5-32.

Taylor, L.A., Neal, C.R. (1989). Eclogites with oceanic crustal and mantle signatures from the Bellsbank kimberlite, South Africa, Part I: mineralogy, petrography, and whole rock chemistry// The Journal of Geology, 97(5), 551-567.

Titus, E., Misra, D.S., Sikder, A.K., Tyagi, P.K., Singh, M.K., Misra, A., Ali, N., Cabral, G., Neto V.F., Gracio, J. (2005). Quantitative analysis of hydrogen in chemical vapor deposited diamond films// Diamond and related materials, 14(3), 476-481.

Tsai, H.M., Meyer, H.O., Moreau, J. Milledge H.J. (1979). Mineral inclusions in diamond: Premier, Jagersfontein and Finsch kimberlites, South Africa, and Williamson mine, Tanzania// Kimberlites, Diatremes, and Diamonds: Their Geology, Petrology and Geochemistry, 16-26.p.

Viljoen, F., Dobbe, R., Smit, B., Thomassot, E., Cartigny, P. (2004). Petrology and geochemistry of a diamondiferous lherzolite from the Premier diamond mine, South Africa// Lithos, 77, 539-552.

Viljoen, F., Dobbe, R., Smit, B. (2009). Geochemical processes in peridotite xenoliths from the Premier diamond mine, South Africa: evidence for the depletion and refertilisation of subcratonic lithosphere// Lithos, 112, 1133-1142.

Viljoen, F., Dobbe, R., Harris J., Smit, B. (2010). Trace element chemistry of mineral inclusions in eclogitic diamonds from the Premier (Cullinan) and Finsch kimberlites, South Africa: Implications for the evolution of their mantle source// Lithos, 118, 156-168.

Wijbrans, C.H., Rohrbach, A., Klemme, S. (2016). An experimental investigation of the stability of majoritic garnet in the Earth's mantle and an improved majorite geobarometer// Contributions to Mineralogy and Petrology, 171(5), 1-20.

References [in the Electronic Supplementary Materials]

Locock, A.J. (2008). An Excel spreadsheet to recast analyses of garnet into end-member components, and a synopsis of the crystal chemistry of natural silicate garnets// Computers & Geosciences, 34(12), 1769-1780.

Locock, A.J. (2014). An Excel spreadsheet to classify chemical analyses of amphiboles following the IMA 2012 recommendations// Computers & Geosciences, 62, 1-11.

Sturm, R. (2002). PX-NOM—an interactive spreadsheet program for the computation of pyroxene analyses derived from the electron microprobe// Computers & Geosciences, 28(4), 473-483.

Appendix A. $\delta^{13}C$ and nitrogen contents in Cullinan diamonds and cathodoluminesence images

*** - spots near inclusions**

Paragenesis	Sample	Inclusions	Spot	Area	$\delta^{13}C$	2σ (‰)	Bulk N (ppm)
Type I							
Sublithospheric mafic	77	Prv	1	core	-2.3	0.5	34
			2*	zone 2	-4.6	0.5	
			3	core	-2.4	0.5	
			4	rim	-3.9	0.5	
			5	rim	-3.9	0.4	
	67	Mj(2) + Omp	1*	core	-3.2	0.5	26
			2*	core	-3.4	0.5	
			3	rim	-5.4	0.5	
	218	Mj(2) + Prp	1*	core	-2.1	0.5	350
			2	zone 2	-4.1	0.5	
			3*	rim	-4.3	0.5	
	297	Mj(2) + Omp	1*	core	-4.2	0.5	45
			2	rim	-4.2	0.5	
	91	Mj	1*	core	-2.9	0.4	77
			2	zone 2	-3.9	0.5	
	101	Mj	1*	core	-4.3	0.5	31
			2	core	-4.1	0.5	
	132	Mj	1	core	-3.4	0.5	22
			2	rim	-4.2	0.4	
	249	Mj	1*	core	-5.3	0.5	220
			2	rim	-3.0	0.5	
	310	Mj	1	core	-4.0	0.5	29
			2*	rim	-4.9	0.5	
			3	zone 2	-4.5	0.4	
Lithospheric eclogitic	145	Grs + Di(2)	1	core	-3.6	0.5	75
			2*	core	-3.5	0.5	
			3	rim	-4.1	0.5	
	106	Prp + Cpx(4)	1	rim	-4.7	0.4	184
			2*	core	-4.6	0.4	
	306	Prp(2) + Omp	1*	core	-4.6	0.5	80
			2	rim	-3.3	0.5	
	195	Prp(2)+Cpx(3)	1*	core	-4.4	0.5	305
			2	rim	-4.6	0.4	
	300	Prp(2) + Omp	1*	core	-4.4	0.5	155
			2	rim	-3.9	0.4	
	314	Prp + Omp(2)	1*	core	-4.7	0.5	720
			2	rim	-4.8	0.5	

Paragenesis	Sample	Inclusions	Spot	Area	$\delta^{13}C$	2σ (‰)	Bulk N (ppm)
Lithospheric eclogitic	68	Prp(4) + Omp	1*	core	-4.5	0.5	285
			2*	core	-4.4	0.5	
			3	rim	-4.1	0.5	
	144	Omp(3)	1*	core	-4.8	0.5	132
			2	rim	-4.5	0.4	
	327	Omp	1*	core	-4.7	0.5	380
			2	rim	-3.9	0.5	
Lithospheric peridotitic	33	Ol	1*	core	-5.0	0.5	133
			2	rim	-4.7	0.5	
	294	Ol(2)	1*	core	-3.1	0.5	53
			2	rim	-2.8	0.5	
	34	Ol	1*	core	-6.4	0.5	155
			2	rim	-7.1	0.5	
	346	Ol	1*	core	-2.8	0.5	40
	334	Ol	1*	core	-7.7	0.5	93
			2	rim	-7.5	0.5	
	227	En(3)	1*	core	-7.5	0.5	193
	276	En	1*	core	-4.6	0.4	470
			2	rim	-5.1	0.5	
Type II							
Sublithospheric mafic	79	Wo	1*	core	-1.8	0.5	8
	85	Mj+Omp	1	core	-4.4	0.4	10
	292	Mj	1	core	-4.3	0.6	4
			2	rim	-4.8	0.5	
	171	Mj+Co(2)+Ky	1*	core	-2.3	0.5	9
	119	Mj	1*	core	-4.1	0.5	17
			2	rim	-4.2	0.5	
	127	Mj	1*	core	-3.6	0.5	12
			2	rim	-4.8	0.5	
	150	Mj	1*	zone 2	-4.7	0.5	20
			2	core	-6.1	0.5	
			3	rim	-4.7	0.5	
Lithospheric eclogitic	8	Co(5)+Ky	1*	core	-2.6	0.5	0
			2	rim	-4.3	0.5	
	62	Omp+Co	1*	core	-3.8	0.5	16
			2	rim	-2.4	0.5	
	181	Omp(2)+Aug	1*	core	-4.2	0.5	12
			2	rim	-4.2	0.5	
	233	Ol(3)	1*	core	-6.8	0.5	4
	341	Ol	1	core	-6.8	0.5	14
			2	rim	-6.7	0.5	
	335	Ol	1*	core	-3.3	0.5	9
			2	core	-3.1	0.5	

Paragenesis	Sample	Inclusions	Spot	Area	$\delta^{13}C$	2σ (‰)	Bulk N (ppm)
Lithospheric peridotitic	51	Ol	1*	core	-7.8	0.5	14
			2	rim	-7.5	0.5	
	125	Ol	1*	core	-3.3	0.4	14
			2	core	-3.1	0.4	
	271	Ol+Prp+En(2)	1*	core	-5.1	0.5	14
			2*	core	-4.8	0.5	
			3	core	-4.7	0.5	
	41	Ol	1*	core	-1.3	0.5	5
			2	rim	-3.8	0.5	
	137	En+Co	1*	core	-2.1	0.5	11
			2	rim	-4.0	0.5	
	318	En(2)+Aug(2)	1*	core	-5.4	0.5	7
			2*	core	-5.6	0.5	
	149	Spl(2)	1*	core	-6.5	0.5	16
			2	rim	-6.4	0.5	

Type-I diamonds. Sublithospheric mafic paragenesis.

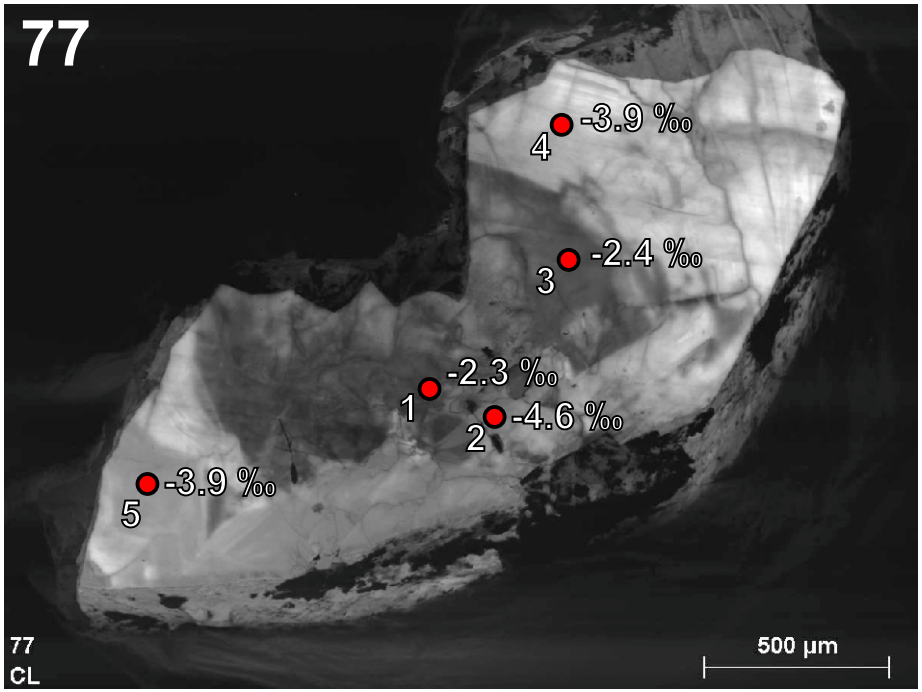

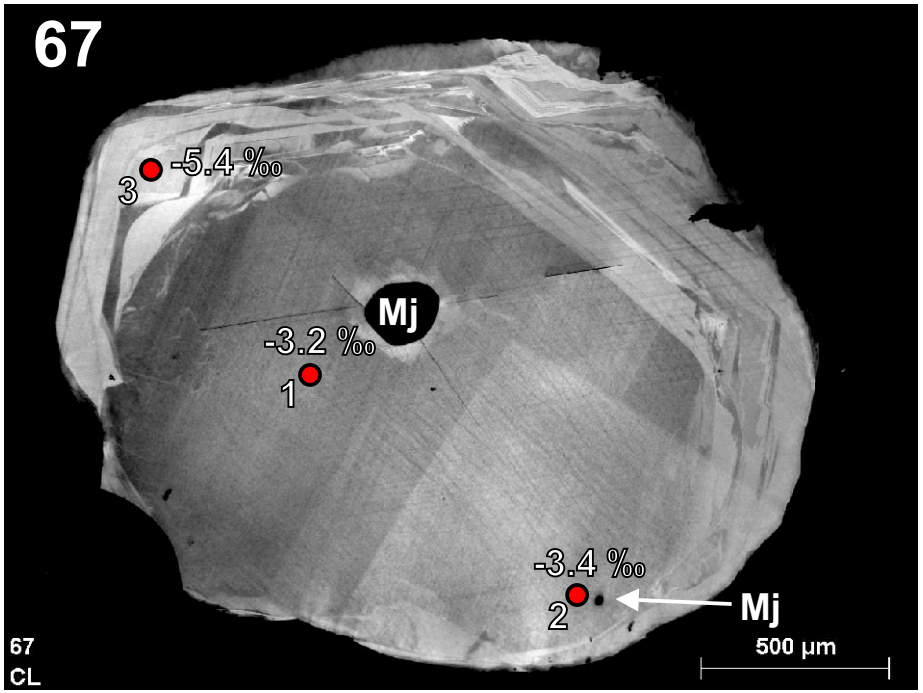

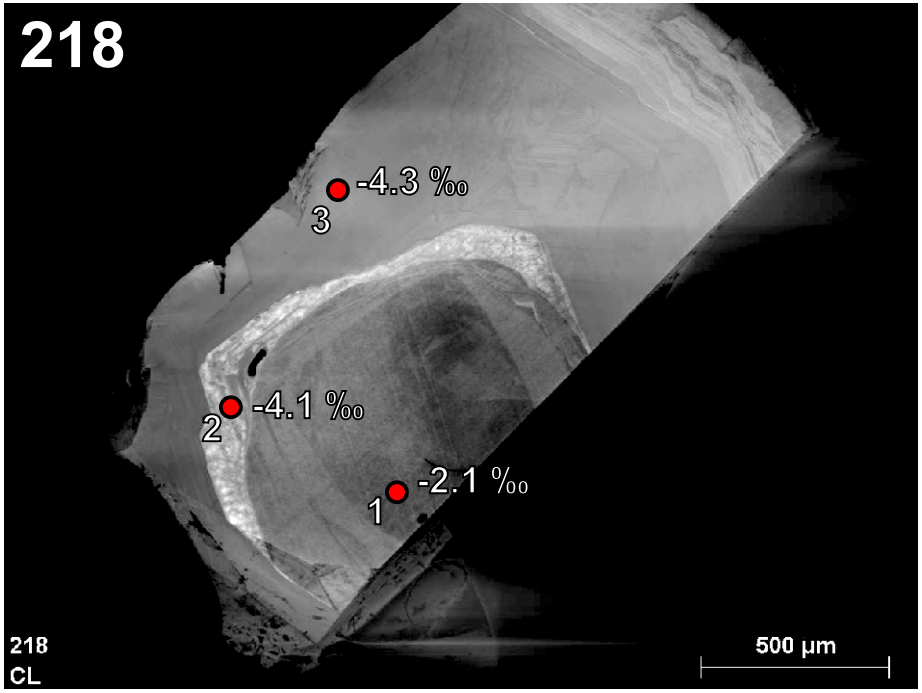

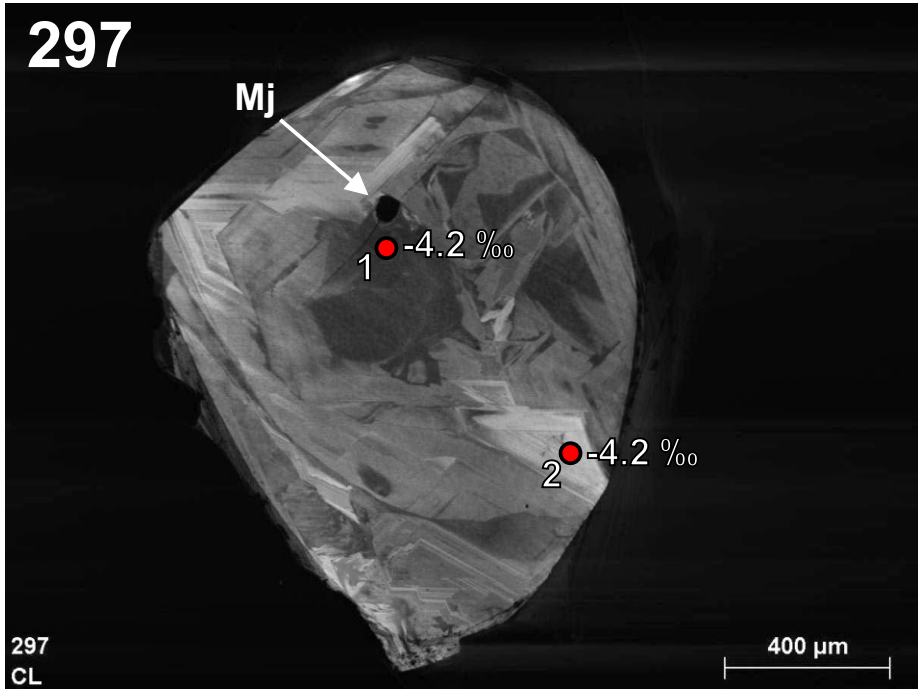

Type-I diamonds. Lithospheric eclogitic paragenesis.

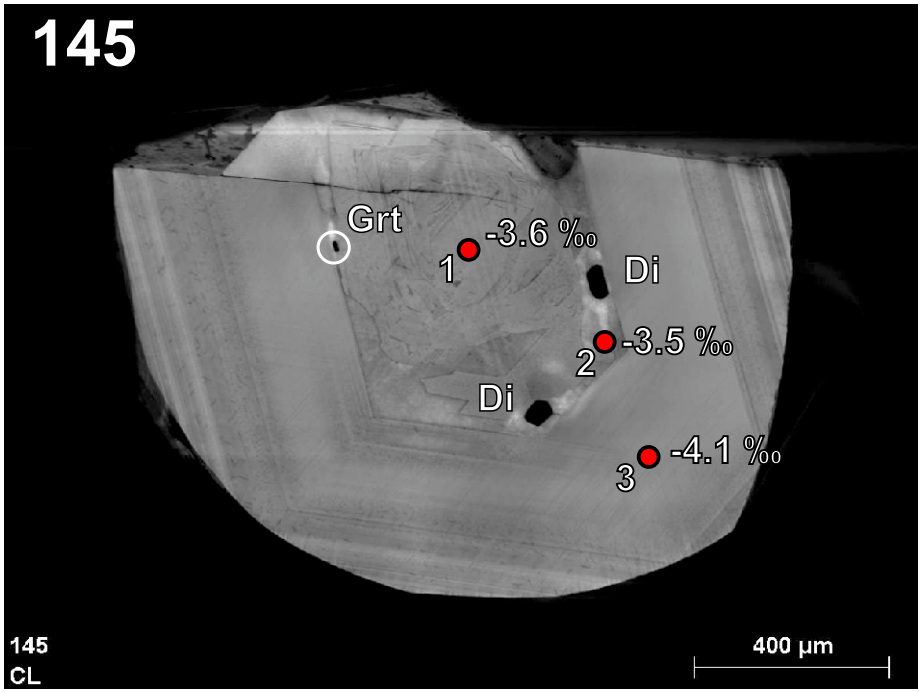

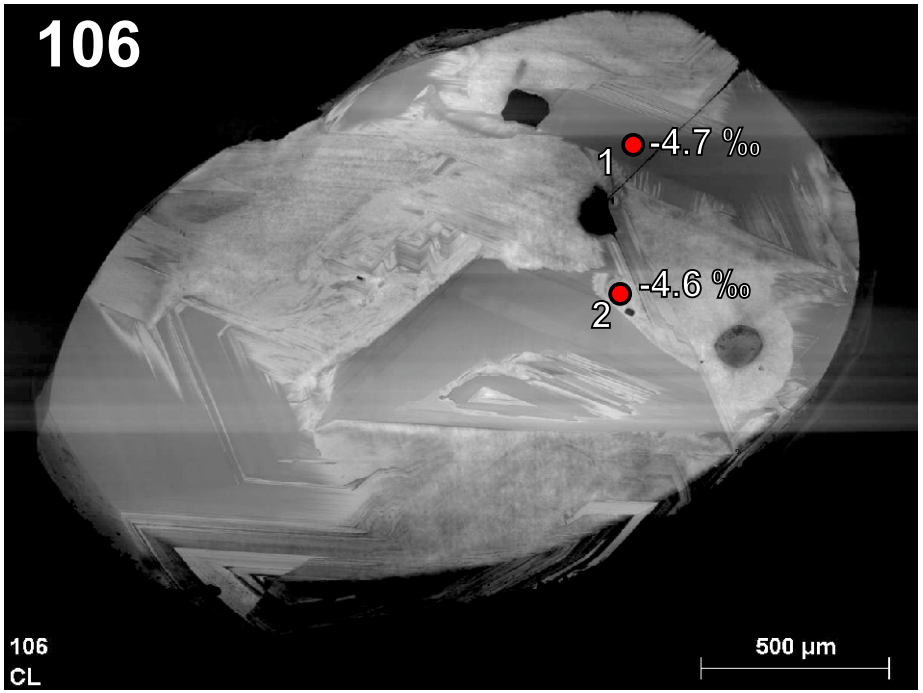

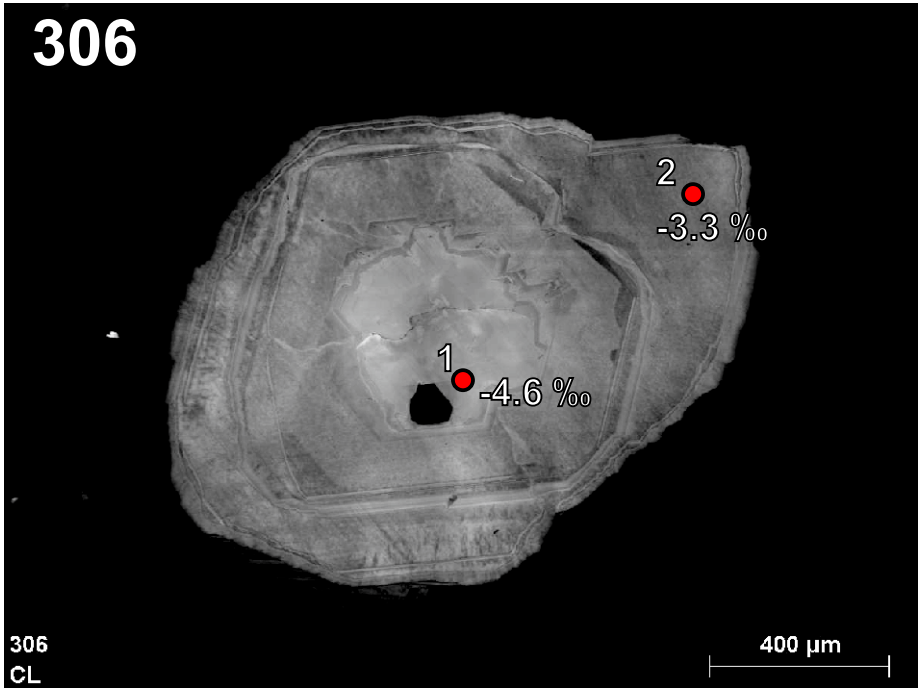

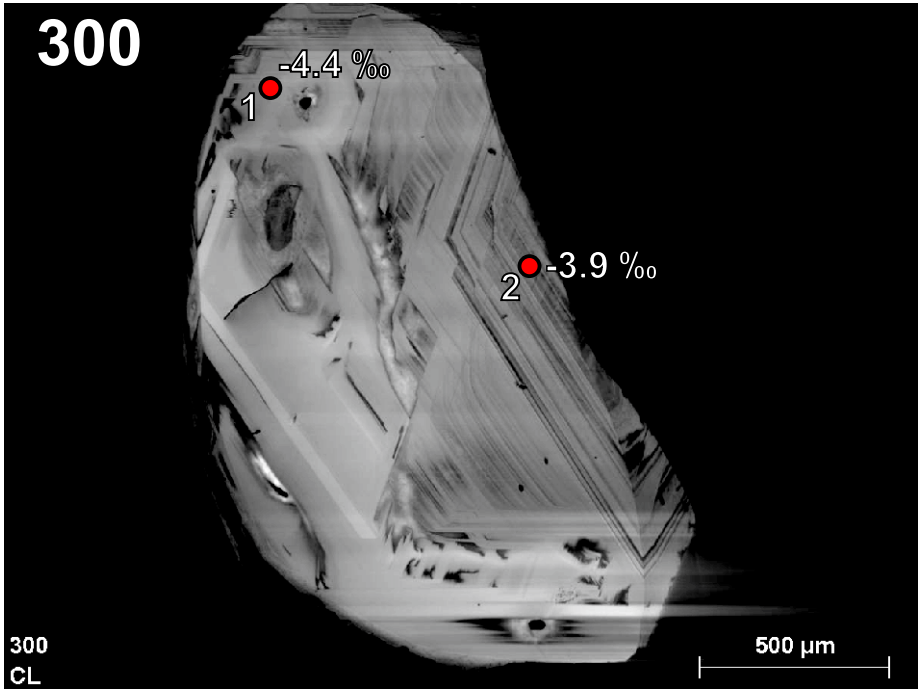

Type-I diamonds. Lithospheric peridotitic paragenesis.

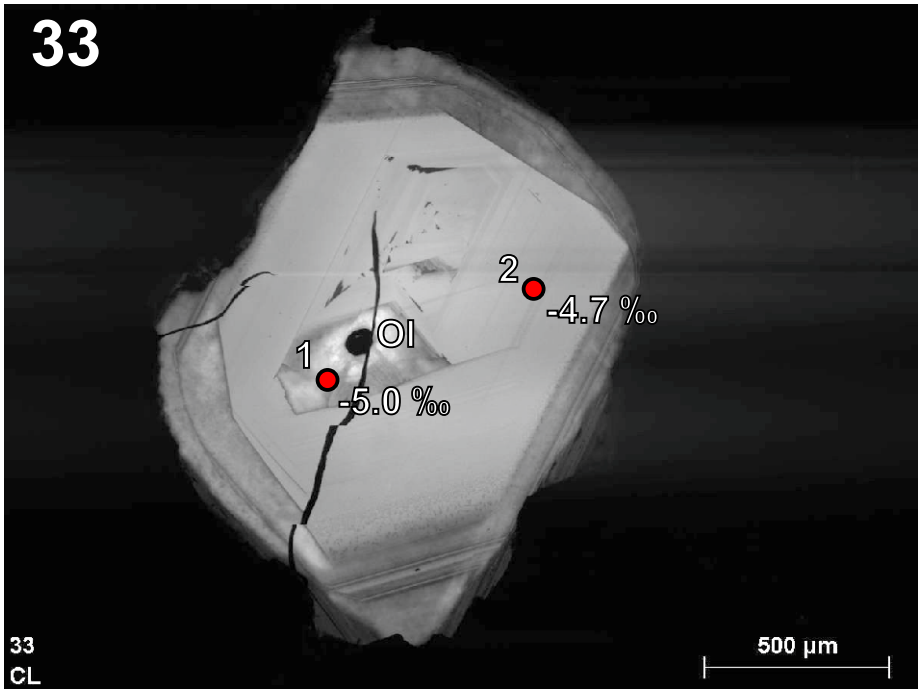

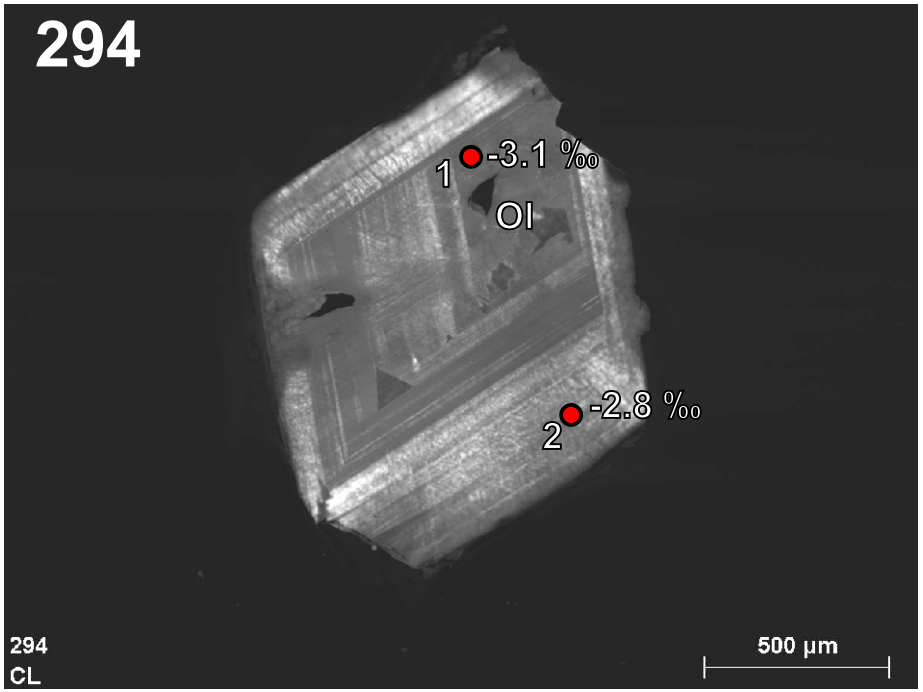

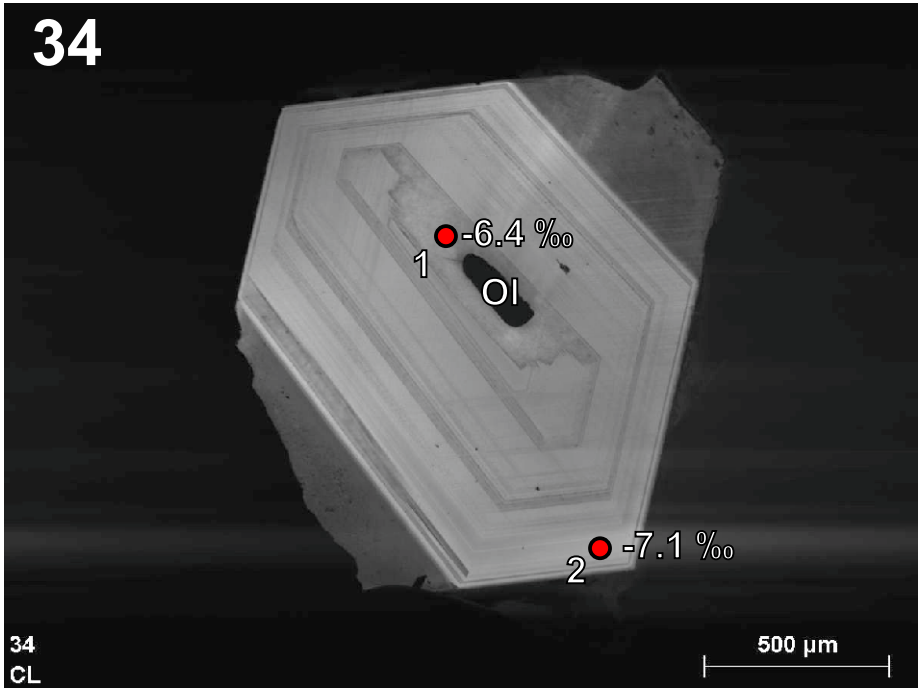

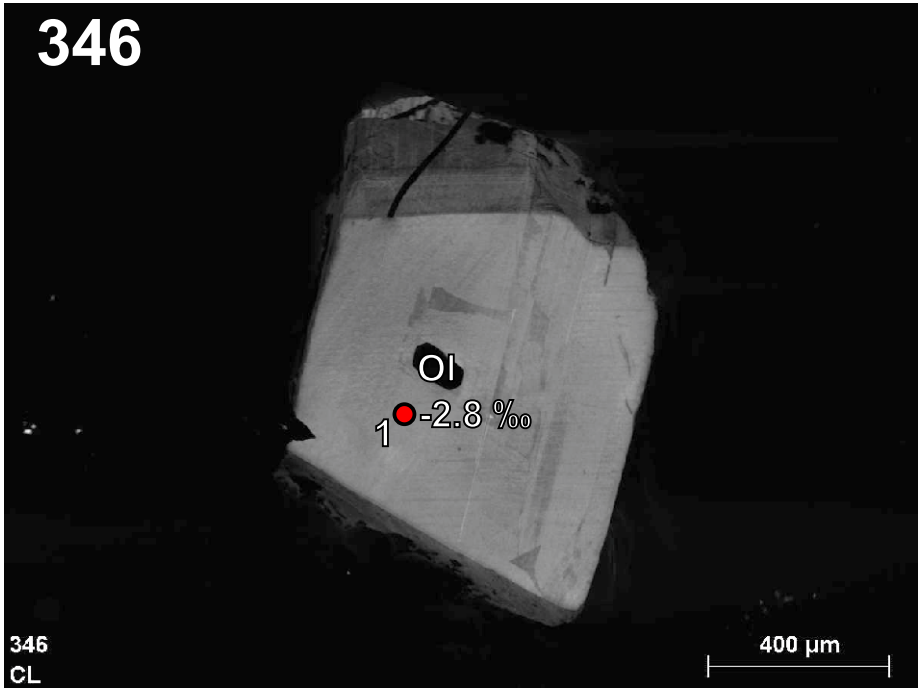

Type-II diamonds. Sublithospheric mafic paragenesis.

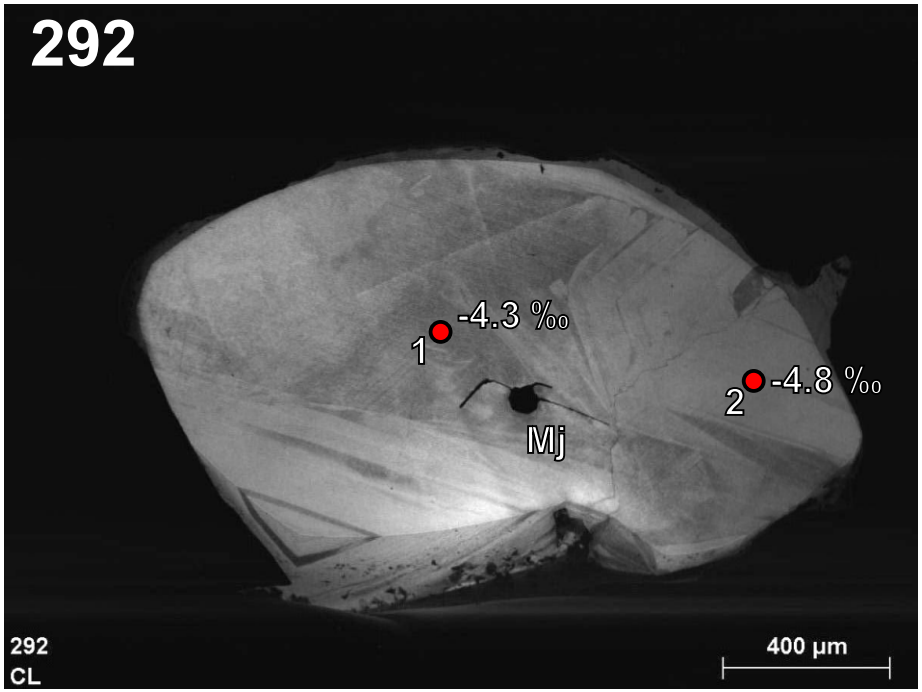

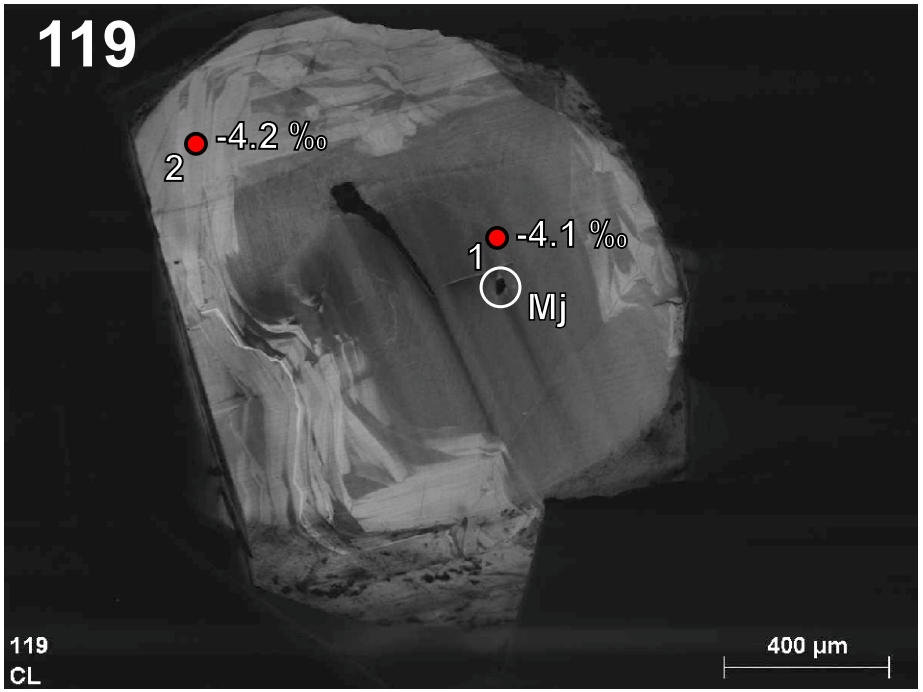

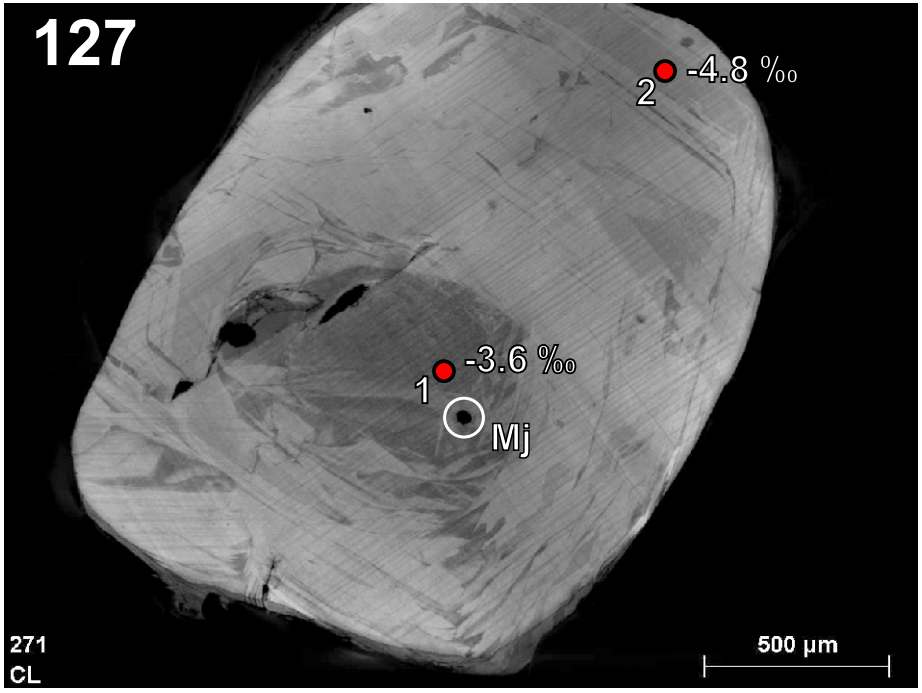

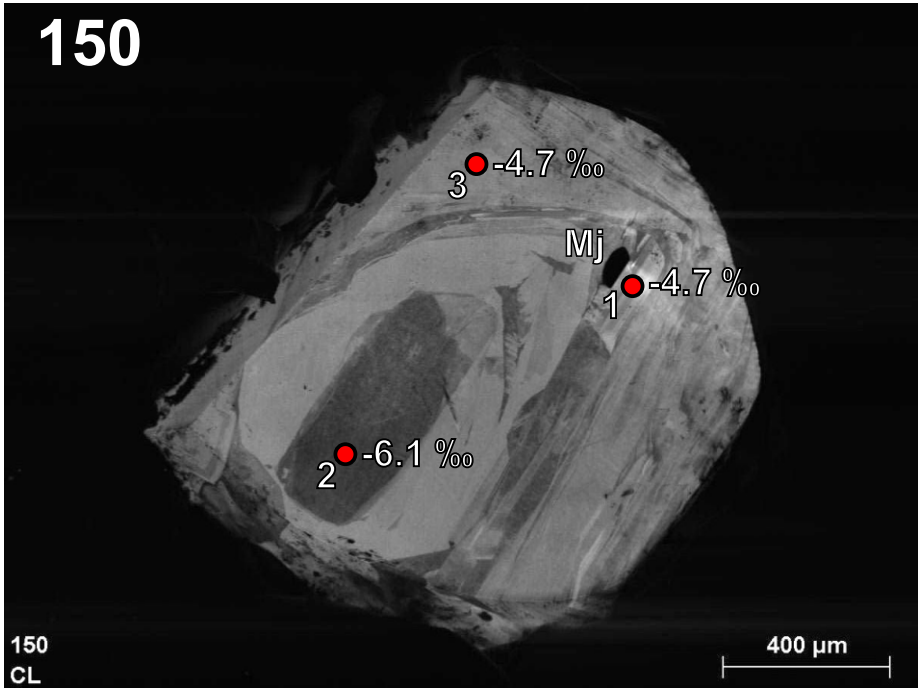

Type-II diamonds. Lithospheric eclogitic paragenesis.

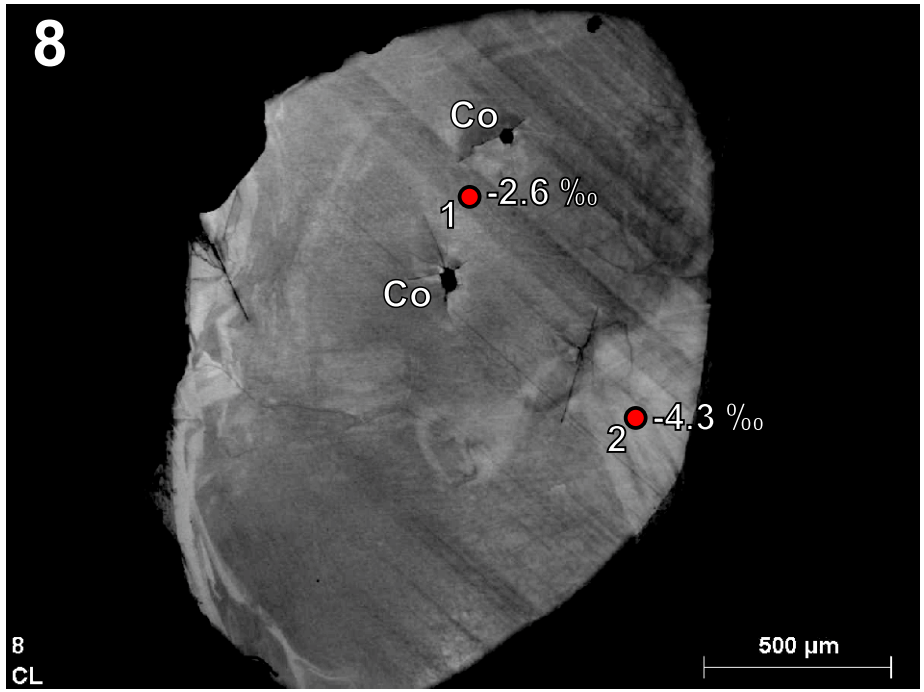

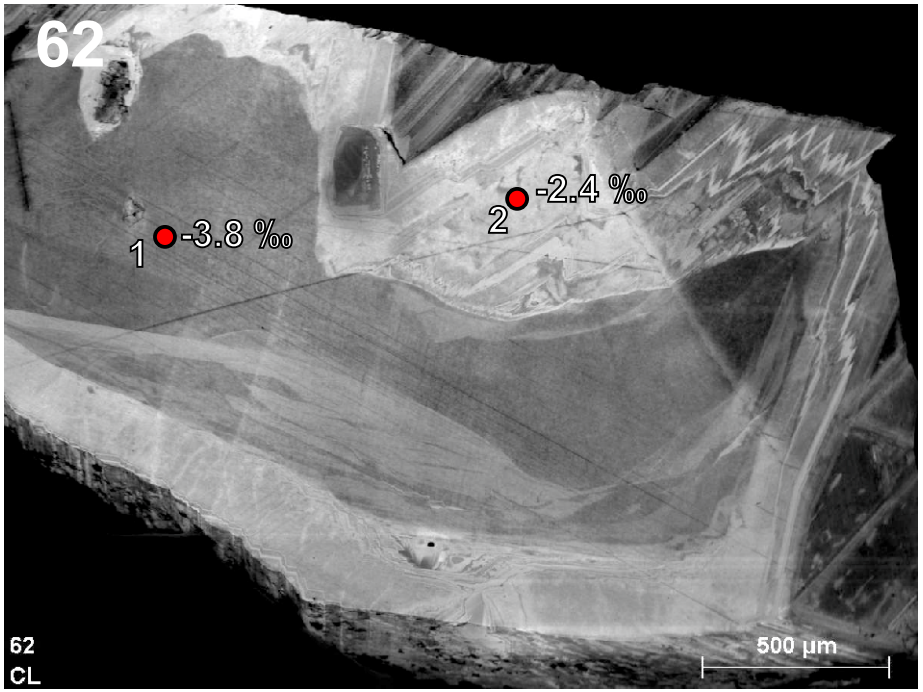

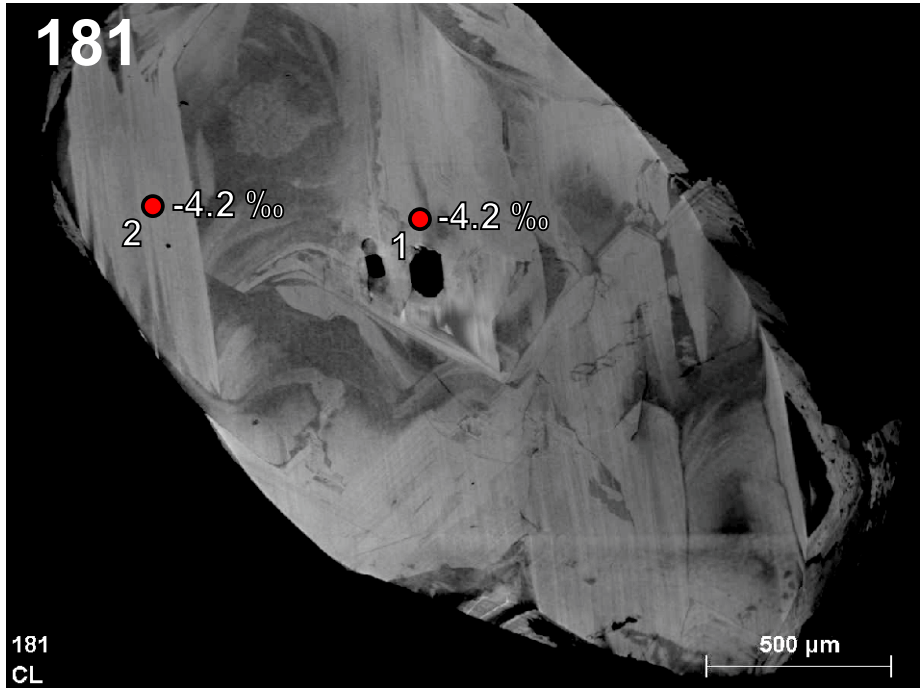

Type-II diamonds. Lithospheric peridotitic paragenesis.